MIKE 21 & MIKE 3 Flow Model FM

Hydrodynamic and Transport Module

Scientific Documentation

DHI headquarters
Agern Allé 5
DK-2970 Hørsholm
Denmark

+45 4516 9200 Telephone
+45 4516 9333 Support
+45 4516 9292 Telefax

mike@dhigroup.com
www.mikepoweredbydhi.com

PLEASE NOTE

COPYRIGHT

This document refers to proprietary computer software, which is protected by copyright. All rights are reserved. Copying or other reproduction of this manual or the related programmes is prohibited without prior written consent of DHI. For details please refer to your 'DHI Software Licence Agreement'.

LIMITED LIABILITY

The liability of DHI is limited as specified in Section III of your 'DHI Software Licence Agreement':

'IN NO EVENT SHALL DHI OR ITS REPRESENTATIVES (AGENTS AND SUPPLIERS) BE LIABLE FOR ANY DAMAGES WHATSOEVER INCLUDING, WITHOUT LIMITATION, SPECIAL, INDIRECT, INCIDENTAL OR CONSEQUENTIAL DAMAGES OR DAMAGES FOR LOSS OF BUSINESS PROFITS OR SAVINGS, BUSINESS INTERRUPTION, LOSS OF BUSINESS INFORMATION OR OTHER PECUNIARY LOSS ARISING OUT OF THE USE OF OR THE INABILITY TO USE THIS DHI SOFTWARE PRODUCT, EVEN IF DHI HAS BEEN ADVISED OF THE POSSIBILITY OF SUCH DAMAGES. THIS LIMITATION SHALL APPLY TO CLAIMS OF PERSONAL INJURY TO THE EXTENT PERMITTED BY LAW. SOME COUNTRIES OR STATES DO NOT ALLOW THE EXCLUSION OR LIMITATION OF LIABILITY FOR CONSEQUENTIAL, SPECIAL, INDIRECT, INCIDENTAL DAMAGES AND, ACCORDINGLY, SOME PORTIONS OF THESE LIMITATIONS MAY NOT APPLY TO YOU. BY YOUR OPENING OF THIS SEALED PACKAGE OR INSTALLING OR USING THE SOFTWARE, YOU HAVE ACCEPTED THAT THE ABOVE LIMITATIONS OR THE MAXIMUM LEGALLY APPLICABLE SUBSET OF THESE LIMITATIONS APPLY TO YOUR PURCHASE OF THIS SOFTWARE.'

CONTENTS

MIKE 21 & MIKE 3 Flow Model FM
Hydrodynamic and Transport Module
Scientific Documentation

1 Introduction

This document presents the scientific background for the new MIKE 21 & MIKE 3 Flow Model FM[1] modelling system developed by DHI Water & Environment. The objective is to provide the user with a detailed description of the flow and transport model equations, numerical discretization and solution methods. Also, model validation is discussed in this document.

The MIKE 21 & MIKE 3 Flow Model FM is based on a flexible mesh approach and it has been developed for applications within oceanographic, coastal and estuarine environments. The modelling system may also be applied for studies of overland flooding.

The system is based on the numerical solution of the two/three-dimensional incompressible Reynolds averaged Navier-Stokes equations invoking the assumptions of Boussinesq and of hydrostatic pressure. Thus, the model consists of continuity, momentum, temperature, salinity and density equations and it is closed by a turbulent closure scheme. For the 3D model the free surface is taken into account using a sigma coordinate transformation approach.

The spatial discretization of the primitive equations is performed using a cell-centred finite volume method. The spatial domain is discretized by subdivision of the continuum into non-overlapping elements/cells. In the horizontal plane, an unstructured grid is used, while in the vertical domain in the 3D model a structured mesh is used. In the 2D model, the elements can be triangles or quadrilateral elements. In the 3D model, the elements can be prisms or bricks, whose horizontal faces are triangles and quadrilateral elements, respectively.

[1] Including the MIKE 21 Flow Model FM (two-dimensional flow) and MIKE 3 Flow Model FM (three-dimensional flow)

2 Governing Equations

2.1 3D Governing Equations in Cartesian Coordinates

2.1.1 Shallow water equations

The model is based on the solution of the three-dimensional incompressible Reynolds averaged Navier-Stokes equations, subject to the assumptions of Boussinesq and of hydrostatic pressure.

The local continuity equation is written as

$$\frac{\partial u}{\partial x}+\frac{\partial v}{\partial y}+\frac{\partial w}{\partial z}=S \tag{2.1}$$

and the two horizontal momentum equations for the x- and y-component, respectively

$$\frac{\partial u}{\partial t}+\frac{\partial u^2}{\partial x}+\frac{\partial vu}{\partial y}+\frac{\partial wu}{\partial z}=fv-g\frac{\partial \eta}{\partial x}-\frac{1}{\rho_0}\frac{\partial p_a}{\partial x}- \frac{g}{\rho_0}\int_z^\eta \frac{\partial \rho}{\partial x}dz-\frac{1}{\rho_0 h}\left(\frac{\partial s_{xx}}{\partial x}+\frac{\partial s_{xy}}{\partial y}\right)+F_u+\frac{\partial}{\partial z}\left(\nu_t\frac{\partial u}{\partial z}\right)+u_sS \tag{2.2}$$

$$\frac{\partial v}{\partial t}+\frac{\partial v^2}{\partial y}+\frac{\partial uv}{\partial x}+\frac{\partial wv}{\partial z}=-fu-g\frac{\partial \eta}{\partial y}-\frac{1}{\rho_0}\frac{\partial p_a}{\partial y}- \frac{g}{\rho_0}\int_z^\eta \frac{\partial \rho}{\partial y}dz-\frac{1}{\rho_0 h}\left(\frac{\partial s_{yx}}{\partial x}+\frac{\partial s_{yy}}{\partial y}\right)+F_v+\frac{\partial}{\partial z}\left(\nu_t\frac{\partial v}{\partial z}\right)+v_sS \tag{2.3}$$

where t is the time; x, y and z are the Cartesian coordinates; η is the surface elevation; d is the still water depth; $h=\eta+d$ is the total water depth; u, v and w are the velocity components in the x, y and z direction; $f=2\Omega\sin\phi$ is the Coriolis parameter (Ω is the angular rate of revolution and ϕ the geographic latitude); g is the gravitational acceleration; ρ is the density of water; s_{xx}, s_{xy}, s_{yx} and s_{yy} are components of the radiation stress tensor; ν_t is the vertical turbulent (or eddy) viscosity; p_a is the atmospheric pressure; ρ_o is the reference density of water. S is the magnitude of the discharge due to point sources and (u_s, v_s) is the velocity by which the water is discharged into the ambient water. The horizontal stress terms are described using a gradient-stress relation, which is simplified to

$$F_u=\frac{\partial}{\partial x}\left(2A\frac{\partial u}{\partial x}\right)+\frac{\partial}{\partial y}\left(A\left(\frac{\partial u}{\partial y}+\frac{\partial v}{\partial x}\right)\right) \tag{2.4}$$

$$F_v = \frac{\partial}{\partial x}\left(A\left(\frac{\partial u}{\partial y} + \frac{\partial v}{\partial x} \right) \right) + \frac{\partial}{\partial y}\left(2A\frac{\partial v}{\partial y} \right) \tag{2.5}$$

where *A* is the horizontal eddy viscosity.

The surface and bottom boundary condition for *u*, *v* and *w* are

At $z = \eta$:

$$\frac{\partial \eta}{\partial t} + u\frac{\partial \eta}{\partial x} + v\frac{\partial \eta}{\partial y} - w = 0, \quad \left(\frac{\partial u}{\partial z}, \frac{\partial v}{\partial z} \right) = \frac{1}{\rho_0 \nu_t}\left(\tau_{sx}, \tau_{sy} \right) \tag{2.6}$$

At $z = -d$:

$$u\frac{\partial d}{\partial x} + v\frac{\partial d}{\partial y} + w = 0, \quad \left(\frac{\partial u}{\partial z}, \frac{\partial v}{\partial z} \right) = \frac{1}{\rho_0 \nu_t}\left(\tau_{bx}, \tau_{by} \right) \tag{2.7}$$

where $\left(\tau_{sx}, \tau_{sy} \right)$ and $\left(\tau_{bx}, \tau_{by} \right)$ are the *x* and *y* components of the surface wind and bottom stresses.

The total water depth, *h*, can be obtained from the kinematic boundary condition at the surface, once the velocity field is known from the momentum and continuity equations. However, a more robust equation is obtained by vertical integration of the local continuity equation

$$\frac{\partial h}{\partial t} + \frac{\partial h\bar{u}}{\partial x} + \frac{\partial h\bar{v}}{\partial y} = hS + \hat{P} - \hat{E} \tag{2.8}$$

where $\hat{P}$ and $\hat{E}$ are precipitation and evaporation rates, respectively, and $\bar{u}$ and $\bar{v}$ are the depth-averaged velocities

$$h\bar{u} = \int_{-d}^{\eta} u dz, \quad h\bar{v} = \int_{-d}^{\eta} v dz \tag{2.9}$$

The fluid is assumed to be incompressible. Hence, the density, ρ, does not depend on the pressure, but only on the temperature, *T*, and the salinity, *s*, via the equation of state

$$\rho = \rho(T, s) \tag{2.10}$$

Here the UNESCO equation of state is used (see UNESCO, 1981).

2.1.2 Transport equations for salt and temperature

The transports of temperature, *T*, and salinity, *s*, follow the general transport-diffusion equations as

$$\frac{\partial T}{\partial t}+\frac{\partial uT}{\partial x}+\frac{\partial vT}{\partial y}+\frac{\partial wT}{\partial z}=F_T+\frac{\partial}{\partial z}\left(D_v\frac{\partial T}{\partial z}\right)+\hat{H}+T_sS \tag{2.11}$$

$$\frac{\partial s}{\partial t}+\frac{\partial us}{\partial x}+\frac{\partial vs}{\partial y}+\frac{\partial ws}{\partial z}=F_s+\frac{\partial}{\partial z}\left(D_v\frac{\partial s}{\partial z}\right)+s_sS \tag{2.12}$$

where D_v is the vertical turbulent (eddy) diffusion coefficient. $\hat{H}$ is a source term due to heat exchange with the atmosphere. T_s and s_s are the temperature and the salinity of the source. *F* are the horizontal diffusion terms defined by

$$\left(F_T,F_s\right)=\left[\frac{\partial}{\partial x}\left(D_h\frac{\partial}{\partial x}\right)+\frac{\partial}{\partial y}\left(D_h\frac{\partial}{\partial y}\right)\right]\left(T,s\right) \tag{2.13}$$

where D_h is the horizontal diffusion coefficient. The diffusion coefficients can be related to the eddy viscosity

$$D_h=\frac{A}{\sigma_T}\quad\text{and}\quad D_v=\frac{\nu_t}{\sigma_T} \tag{2.14}$$

where σ_T is the Prandtl number. In many applications a constant Prandtl number can be used (see Rodi (1984)).

The surface and bottom boundary conditions for the temperature are

At $z=\eta$:

$$D_h\frac{\partial T}{\partial z}=\frac{Q_n}{\rho_0c_p}+T_p\hat{P}-T_e\hat{E} \tag{2.15}$$

At $z=-d$:

$$\frac{\partial T}{\partial z}=0 \tag{2.16}$$

where Q_n is the surface net heat flux and $c_p=4217\ J/(kg\cdot°K)$ is the specific heat of the water. A detailed description for determination of $\hat{H}$ and Q_n is given in Section 2.10.

The surface and bottom boundary conditions for the salinity are

At $z = \eta$:

$$\frac{\partial s}{\partial z} = 0 \tag{2.17}$$

At $z = -d$:

$$\frac{\partial s}{\partial z} = 0 \tag{2.18}$$

When heat exchange from the atmosphere is included, the evaporation is defined as

$$\hat{E} = \begin{cases} \dfrac{q_v}{\rho_0 l_v} & q_v > 0 \\ 0 & q_v \le 0 \end{cases} \tag{2.19}$$

where q_v is the latent heat flux and $l_v = 2.5 \cdot 10^6$ is the latent heat of vaporisation of water.

2.1.3 Transport equation for a scalar quantity

The conservation equation for a scalar quantity is given by

$$\frac{\partial C}{\partial t} + \frac{\partial uC}{\partial x} + \frac{\partial vC}{\partial y} + \frac{\partial wC}{\partial z} = F_C + \frac{\partial}{\partial z}\left(D_v \frac{\partial C}{\partial z} \right) - k_p C + C_s S \tag{2.20}$$

where *C* is the concentration of the scalar quantity, k_p is the linear decay rate of the scalar quantity, C_s is the concentration of the scalar quantity at the source and D_v is the vertical diffusion coefficient. F_C is the horizontal diffusion term defined by

$$F_C = \left[\frac{\partial}{\partial x}\left(D_h \frac{\partial}{\partial x} \right) + \frac{\partial}{\partial y}\left(D_h \frac{\partial}{\partial y} \right) \right] C \tag{2.21}$$

where D_h is the horizontal diffusion coefficient.

2.1.4 Turbulence model

The turbulence is modelled using an eddy viscosity concept. The eddy viscosity is often described separately for the vertical and the horizontal transport. Here several turbulence models can be applied: a constant viscosity, a vertically parabolic viscosity and a standard k-ε model (Rodi, 1984). In many numerical simulations the small-scale turbulence cannot be resolved with the chosen spatial resolution. This kind of turbulence can be approximated using sub-grid scale models.

Vertical eddy viscosity

The eddy viscosity derived from the log-law is calculated by

$$\nu_t = U_\tau h\left(c_1\frac{z+d}{h}+c_2\left(\frac{z+d}{h}\right)^2\right) \tag{2.22}$$

where $U_\tau = \max(U_{\tau s}, U_{\tau b})$ and c_1 and c_2 are two constants. $U_{\tau s}$ and $U_{\tau b}$ are the friction velocities associated with the surface and bottom stresses, $c_1 = 0.41$ and $c_2 = -0.41$ give the standard parabolic profile.

In applications with stratification the effects of buoyancy can be included explicitly. This is done through the introduction of a Richardson number dependent damping of the eddy viscosity coefficient, when a stable stratification occurs. The damping is a generalisation of the Munk-Anderson formulation (Munk and Anderson, 1948)

$$\nu_t = \nu_t^*(1+aRi)^{-b} \tag{2.23}$$

where ν_t^* is the undamped eddy viscosity and *Ri* is the local gradient Richardson number

$$Ri = -\frac{g}{\rho_0}\frac{\partial\rho}{\partial z}\left(\left(\frac{\partial u}{\partial z}\right)^2+\left(\frac{\partial v}{\partial z}\right)^2\right)^{-1} \tag{2.24}$$

$a = 10$ and $b = 0.5$ are empirical constants.

In the k-ε model the eddy-viscosity is derived from turbulence parameters *k* and ε as

$$\nu_t = c_\mu\frac{k^2}{\varepsilon} \tag{2.25}$$

where *k* is the turbulent kinetic energy per unit mass (TKE), ε is the dissipation of TKE and c_μ is an empirical constant.

The turbulent kinetic energy, *k,* and the dissipation of TKE, ε, are obtained from the following transport equations

$$\frac{\partial k}{\partial t}+\frac{\partial uk}{\partial x}+\frac{\partial vk}{\partial y}+\frac{\partial wk}{\partial z} = F_k+\frac{\partial}{\partial z}\left(\frac{\nu_t}{\sigma_k}\frac{\partial k}{\partial z}\right)+P+B-\varepsilon \tag{2.26}$$

$$\frac{\partial\varepsilon}{\partial t}+\frac{\partial u\varepsilon}{\partial x}+\frac{\partial v\varepsilon}{\partial y}+\frac{\partial w\varepsilon}{\partial z} = F_\varepsilon+\frac{\partial}{\partial z}\left(\frac{\nu_t}{\sigma_\varepsilon}\frac{\partial\varepsilon}{\partial z}\right)+\frac{\varepsilon}{k}\left(c_{1\varepsilon}P+c_{3\varepsilon}B-c_{2\varepsilon}\varepsilon\right) \tag{2.27}$$

where the shear production, *P*, and the buoyancy production, *B*, are given as

$$P = \frac{\tau_{xz}}{\rho_0}\frac{\partial u}{\partial z} + \frac{\tau_{yz}}{\rho_0}\frac{\partial v}{\partial z} \approx \nu_t\left(\left(\frac{\partial u}{\partial z}\right)^2 + \left(\frac{\partial v}{\partial z}\right)^2\right) \tag{2.28}$$

$$B = -\frac{\nu_t}{\sigma_t}N^2 \tag{2.29}$$

with the Brunt-Väisälä frequency, *N*, defined by

$$N^2 = -\frac{g}{\rho_0}\frac{\partial \rho}{\partial z} \tag{2.30}$$

σ_t is the turbulent Prandtl number and σ_k , σ_ε, $c_{1\varepsilon}$, $c_{2\varepsilon}$ and $c_{3\varepsilon}$ are empirical constants. *F* are the horizontal diffusion terms defined by

$$(F_k, F_\varepsilon) = \left[\frac{\partial}{\partial x}\left(D_h\frac{\partial}{\partial x}\right) + \frac{\partial}{\partial y}\left(D_h\frac{\partial}{\partial y}\right)\right](k, \varepsilon) \tag{2.31}$$

The horizontal diffusion coefficients are given by $D_h = A/\sigma_k$ and $D_h = A/\sigma_\varepsilon$, respectively.

Several carefully calibrated empirical coefficients enter the k-e turbulence model. The empirical constants are listed in (2.47) (see Rodi, 1984).

Table 2.1 Empirical constants in the k-ε model.

c_μ	$c_{1\varepsilon}$	$c_{2\varepsilon}$	$c_{3\varepsilon}$	σ_t	σ_k	σ_ε
0.09	1.44	1.92	0	0.9	1.0	1.3

At the surface the boundary conditions for the turbulent kinetic energy and its rate of dissipation depend on the wind shear, $U_{\tau s}$

At $z = \eta$:

$$k = \frac{1}{\sqrt{c_\mu}}U_{\tau s}^2 \tag{2.32}$$

$$\varepsilon = \frac{U_{\tau s}^3}{\kappa \Delta z_b} \qquad \text{for} \quad U_{\tau s} > 0$$

$$\frac{\partial k}{\partial z} = 0 \qquad \varepsilon = \frac{\left(k\sqrt{c_\mu}\right)^{3/2}}{a\kappa h} \qquad \text{for} \quad U_{\tau s} = 0 \tag{2.33}$$

where κ=0.4 is the von Kármán constant, $a = 0.07$ is and empirical constant and Δz_s is the distance from the surface where the boundary condition is imposed. At the seabed the boundary conditions are

At $z = -d$:

$$k = \frac{1}{\sqrt{c_\mu}} U_{\tau b}^2 \qquad \varepsilon = \frac{U_{\tau b}^3}{\kappa \Delta z_b} \tag{2.34}$$

where Δz_b is the distance from the bottom where the boundary condition is imposed.

Horizontal eddy viscosity

In many applications a constant eddy viscosity can be used for the horizontal eddy viscosity. Alternatively, Smagorinsky (1963) proposed to express sub-grid scale transports by an effective eddy viscosity related to a characteristic length scale. The subgrid scale eddy viscosity is given by

$$A = c_s^2 l^2 \sqrt{2 S_{ij} S_{ij}} \tag{2.35}$$

where c_s is a constant, l is a characteristic length and the deformation rate is given by

$$S_{ij} = \frac{1}{2}\left(\frac{\partial u_i}{\partial x_j} + \frac{\partial u_j}{\partial x_i} \right) \quad (i, j = 1,2) \tag{2.36}$$

2.1.5 Governing equations in Cartesian and sigma coordinates

The equations are solved using a vertical σ-transformation

$$\sigma = \frac{z - z_b}{h}, \quad x' = x, \quad y' = y \tag{2.37}$$

where σ varies between 0 at the bottom and 1 at the surface. The coordinate transformation implies relations such as

$$\frac{\partial}{\partial z} = \frac{1}{h}\frac{\partial}{\partial \sigma} \tag{2.38}$$

$$\left(\frac{\partial}{\partial x}, \frac{\partial}{\partial y} \right) = \left(\frac{\partial}{\partial x'} - \frac{1}{h}\left(-\frac{\partial d}{\partial x} + \sigma \frac{\partial h}{\partial x} \right) \frac{\partial}{\partial \sigma}, \frac{\partial}{\partial y'} - \frac{1}{h}\left(-\frac{\partial d}{\partial y} + \sigma \frac{\partial h}{\partial y} \right) \frac{\partial}{\partial \sigma} \right) \tag{2.39}$$

In this new coordinate system the governing equations are given as

$$\frac{\partial h}{\partial t} + \frac{\partial hu}{\partial x'} + \frac{\partial hv}{\partial y'} + \frac{\partial h\omega}{\partial \sigma} = hS \tag{2.40}$$

$$\frac{\partial hu}{\partial t}+\frac{\partial hu^2}{\partial x'}+\frac{\partial hvu}{\partial y'}+\frac{\partial h\omega u}{\partial \sigma}=fvh-gh\frac{\partial \eta}{\partial x'}-\frac{h}{\rho_0}\frac{\partial p_a}{\partial x'}-\frac{hg}{\rho_0}\int_z^\eta \frac{\partial \rho}{\partial x}dz-\frac{1}{\rho_0}\left(\frac{\partial s_{xx}}{\partial x}+\frac{\partial s_{xy}}{\partial y}\right)+hF_u+\frac{\partial}{\partial \sigma}\left(\frac{\nu_v}{h}\frac{\partial u}{\partial \sigma}\right)+hu_sS \quad (2.41)$$

$$\frac{\partial hv}{\partial t}+\frac{\partial huv}{\partial x'}+\frac{\partial hv^2}{\partial y'}+\frac{\partial h\omega v}{\partial \sigma}=-fuh-gh\frac{\partial \eta}{\partial y'}-\frac{h}{\rho_0}\frac{\partial p_a}{\partial y'}-\frac{hg}{\rho_0}\int_z^\eta \frac{\partial \rho}{\partial y}dz-\frac{1}{\rho_0}\left(\frac{\partial s_{yx}}{\partial x}+\frac{\partial s_{yy}}{\partial y}\right)+hF_v+\frac{\partial}{\partial \sigma}\left(\frac{\nu_v}{h}\frac{\partial v}{\partial \sigma}\right)+hv_sS \quad (2.42)$$

$$\frac{\partial hT}{\partial t}+\frac{\partial huT}{\partial x'}+\frac{\partial hvT}{\partial y'}+\frac{\partial h\omega T}{\partial \sigma}=hF_T+\frac{\partial}{\partial \sigma}\left(\frac{D_v}{h}\frac{\partial T}{\partial \sigma}\right)+h\hat{H}+hT_sS \quad (2.43)$$

$$\frac{\partial hs}{\partial t}+\frac{\partial hus}{\partial x'}+\frac{\partial hvs}{\partial y'}+\frac{\partial h\omega s}{\partial \sigma}=hF_s+\frac{\partial}{\partial \sigma}\left(\frac{D_v}{h}\frac{\partial s}{\partial \sigma}\right)+hs_sS \quad (2.44)$$

$$\frac{\partial hk}{\partial t}+\frac{\partial huk}{\partial x'}+\frac{\partial hvk}{\partial y'}+\frac{\partial h\omega k}{\partial \sigma}=hF_k+\frac{1}{h}\frac{\partial}{\partial \sigma}\left(\frac{\nu_t}{\sigma_k}\frac{\partial k}{\partial \sigma}\right)+h(P+B-\varepsilon) \quad (2.45)$$

$$\frac{\partial h\varepsilon}{\partial t}+\frac{\partial hu\varepsilon}{\partial x'}+\frac{\partial hv\varepsilon}{\partial y'}+\frac{\partial h\omega \varepsilon}{\partial \sigma}=hF_\varepsilon+\frac{1}{h}\frac{\partial}{\partial \sigma}\left(\frac{\nu_t}{\sigma_\varepsilon}\frac{\partial \varepsilon}{\partial \sigma}\right)+h\frac{\varepsilon}{k}\left(c_{1\varepsilon}P+c_{3\varepsilon}B-c_{2\varepsilon}\varepsilon\right) \quad (2.46)$$

$$\frac{\partial hC}{\partial t}+\frac{\partial huC}{\partial x'}+\frac{\partial hvC}{\partial y'}+\frac{\partial h\omega C}{\partial \sigma}=hF_C+\frac{\partial}{\partial \sigma}\left(\frac{D_v}{h}\frac{\partial C}{\partial \sigma}\right)-hk_pC+hC_sS \quad (2.47)$$

The modified vertical velocity is defined by

$$\omega=\frac{1}{h}\left[w+u\frac{\partial d}{\partial x'}+v\frac{\partial d}{\partial y'}-\sigma\left(\frac{\partial h}{\partial t}+u\frac{\partial h}{\partial x'}+v\frac{\partial h}{\partial y'}\right)\right] \quad (2.48)$$

The modified vertical velocity is the velocity across a level of constant σ. The horizontal diffusion terms are defined as

$$hF_u\approx\frac{\partial}{\partial x}\left(2hA\frac{\partial u}{\partial x}\right)+\frac{\partial}{\partial y}\left(hA\left(\frac{\partial u}{\partial y}+\frac{\partial v}{\partial x}\right)\right) \quad (2.49)$$

$$hF_v\approx\frac{\partial}{\partial x}\left(hA\left(\frac{\partial u}{\partial y}+\frac{\partial v}{\partial x}\right)\right)+\frac{\partial}{\partial y}\left(2hA\frac{\partial v}{\partial y}\right) \quad (2.50)$$

$$h(F_T, F_s, F_k, F_\varepsilon, F_c) \approx \left[\frac{\partial}{\partial x}\left(hD_h\frac{\partial}{\partial x}\right)+\frac{\partial}{\partial y}\left(hD_h\frac{\partial}{\partial y}\right)\right](T, s, k, \varepsilon, C) \tag{2.51}$$

The boundary condition at the free surface and at the bottom are given as follows

At σ =1:

$$\omega = 0, \quad \left(\frac{\partial u}{\partial \sigma}, \frac{\partial v}{\partial \sigma}\right) = \frac{h}{\rho_0 \nu_t}\left(\tau_{sx}, \tau_{sy}\right) \tag{2.52}$$

At σ =0:

$$\omega = 0, \quad \left(\frac{\partial u}{\partial \sigma}, \frac{\partial v}{\partial \sigma}\right) = \frac{h}{\rho_0 \nu_t}\left(\tau_{bx}, \tau_{by}\right) \tag{2.53}$$

The equation for determination of the water depth is not changed by the coordinate transformation. Hence, it is identical to Eq. (2.6).

2.2 3D Governing Equations in Spherical and Sigma Coordinates

In spherical coordinates the independent variables are the longitude, λ , and the latitude, ϕ . The horizontal velocity field (*u,v*) is defined by

$$u = R\cos\phi\frac{d\lambda}{dt} \qquad v = R\frac{d\phi}{dt} \tag{2.54}$$

where *R* is the radius of the earth.

In this coordinate system the governing equations are given as (all superscripts indicating the horizontal coordinate in the new coordinate system are dropped in the following for notational convenience)

$$\frac{\partial h}{\partial t}+\frac{1}{R\cos\phi}\left(\frac{\partial hu}{\partial \lambda}+\frac{\partial hv\cos\phi}{\partial \phi}\right)+\frac{\partial h\omega}{\partial \sigma} = hS \tag{2.55}$$

$$\frac{\partial hu}{\partial t}+\frac{1}{R\cos\phi}\left(\frac{\partial hu^2}{\partial \lambda}+\frac{\partial hvu\cos\phi}{\partial \phi}\right)+\frac{\partial h\omega u}{\partial \sigma} = \left(f+\frac{u}{R}\tan\phi\right)vh - \frac{1}{R\cos\phi}\left(gh\frac{\partial \eta}{\partial \lambda}+\frac{1}{\rho_0}\frac{\partial p_a}{\partial \lambda}+\frac{g}{\rho_0}\int_z^\eta \frac{\partial \rho}{\partial \lambda}dz+\frac{1}{\rho_0}\left(\frac{\partial s_{xx}}{\partial \lambda}+\cos\phi\frac{\partial s_{xy}}{\partial \phi}\right)\right)+ hF_u+\frac{\partial}{\partial \sigma}\left(\frac{\nu_v}{h}\frac{\partial u}{\partial \sigma}\right)+hu_sS \tag{2.56}$$

$$\frac{\partial hv}{\partial t}+\frac{1}{R\cos\phi}\left(\frac{\partial huv}{\partial\lambda}+\frac{\partial hv^2\cos\phi}{\partial\phi}\right)+\frac{\partial h\omega v}{\partial\sigma}=-\left(f+\frac{u}{R}\tan\phi\right)uh-$$
$$\frac{1}{R}\left(gh\frac{\partial\eta}{\partial\phi}+\frac{1}{\rho_0}\frac{\partial p_a}{\partial\phi}+\frac{g}{\rho_0}\int_z^\eta\frac{\partial\rho}{\partial\phi}dz+\frac{1}{\rho_0}\left(\frac{1}{\cos\phi}\frac{\partial s_{yx}}{\partial\lambda}+\frac{\partial s_{yy}}{\partial\phi}\right)\right)+ \quad (2.57)$$
$$hF_v+\frac{\partial}{\partial\sigma}\left(\frac{\nu_v}{h}\frac{\partial v}{\partial\sigma}\right)+hv_sS$$

$$\frac{\partial hT}{\partial t}+\frac{1}{R\cos\phi}\left(\frac{\partial huT}{\partial\lambda}+\frac{\partial hvT\cos\phi}{\partial\phi}\right)+\frac{\partial h\omega T}{\partial\sigma}= \quad (2.58)$$
$$hF_T+\frac{\partial}{\partial\sigma}\left(\frac{D_v}{h}\frac{\partial T}{\partial\sigma}\right)+h\widehat{H}+hT_sS$$

$$\frac{\partial hs}{\partial t}+\frac{1}{R\cos\phi}\left(\frac{\partial hus}{\partial\lambda}+\frac{\partial hvs\cos\phi}{\partial\phi}\right)+\frac{\partial h\omega s}{\partial\sigma}= \quad (2.59)$$
$$hF_s+\frac{\partial}{\partial\sigma}\left(\frac{D_v}{h}\frac{\partial s}{\partial\sigma}\right)+hs_sS$$

$$\frac{\partial hk}{\partial t}+\frac{1}{R\cos\phi}\left(\frac{\partial huk}{\partial\lambda}+\frac{\partial hvk\cos\phi}{\partial\phi}\right)+\frac{\partial h\omega k}{\partial\sigma}= \quad (2.60)$$
$$hF_k+\frac{1}{h}\frac{\partial}{\partial\sigma}\left(\frac{\nu_t}{\sigma_k}\frac{\partial k}{\partial\sigma}\right)+h(P+B-\varepsilon)$$

$$\frac{\partial h\varepsilon}{\partial t}+\frac{1}{R\cos\phi}\left(\frac{\partial hu\varepsilon}{\partial\lambda}+\frac{\partial hv\varepsilon\cos\phi}{\partial\phi}\right)+\frac{\partial h\omega\varepsilon}{\partial\sigma}= \quad (2.61)$$
$$hF_\varepsilon+\frac{1}{h}\frac{\partial}{\partial\sigma}\left(\frac{\nu_t}{\sigma_\varepsilon}\frac{\partial\varepsilon}{\partial\sigma}\right)+h\frac{\varepsilon}{k}\left(c_{1\varepsilon}P+c_{3\varepsilon}B-c_{2\varepsilon}\varepsilon\right)$$

$$\frac{\partial hC}{\partial t}+\frac{1}{R\cos\phi}\left(\frac{\partial huC}{\partial\lambda}+\frac{\partial hvC\cos\phi}{\partial\phi}\right)+\frac{\partial h\omega C}{\partial\sigma}= \quad (2.62)$$
$$hF_C+\frac{\partial}{\partial\sigma}\left(\frac{D_v}{h}\frac{\partial C}{\partial\sigma}\right)-hk_pC+hC_sS$$

The modified vertical velocity in spherical coordinates is defined by

$$\omega=\frac{1}{h}\left[w+\frac{u}{R\cos\phi}\frac{\partial d}{\partial\lambda}+\frac{v}{R}\frac{\partial d}{\partial y}-\sigma\left(\frac{\partial h}{\partial t}+\frac{u}{R\cos\phi}\frac{\partial h}{\partial\lambda}+\frac{v}{R}\frac{\partial h}{\partial\phi}\right)\right] \quad (2.63)$$

The equation determining the water depth in spherical coordinates is given as

$$\frac{\partial h}{\partial t}+\frac{1}{R\cos\phi}\left(\frac{\partial h\bar{u}}{\partial\lambda}+\frac{\partial h\bar{v}\cos\phi}{\partial\phi}\right)=hS \quad (2.64)$$

2.3 2D Governing Equations in Cartesian Coordinates

2.3.1 Shallow water equations

Integration of the horizontal momentum equations and the continuity equation over depth $h = \eta + d$ the following two-dimensional shallow water equations are obtained

$$\frac{\partial h}{\partial t} + \frac{\partial h\bar{u}}{\partial x} + \frac{\partial h\bar{v}}{\partial y} = hS \tag{2.65}$$

$$\begin{aligned}\frac{\partial h\bar{u}}{\partial t} + \frac{\partial h\bar{u}^2}{\partial x} + \frac{\partial h\bar{v}\bar{u}}{\partial y} = {} & f\bar{v}h - gh\frac{\partial \eta}{\partial x} - \frac{h}{\rho_0}\frac{\partial p_a}{\partial x} - \\ & \frac{gh^2}{2\rho_0}\frac{\partial \rho}{\partial x} + \frac{\tau_{sx}}{\rho_0} - \frac{\tau_{bx}}{\rho_0} - \frac{1}{\rho_0}\left(\frac{\partial s_{xx}}{\partial x} + \frac{\partial s_{xy}}{\partial y}\right) + \\ & \frac{\partial}{\partial x}\left(hT_{xx}\right) + \frac{\partial}{\partial y}\left(hT_{xy}\right) + hu_s S\end{aligned} \tag{2.66}$$

$$\begin{aligned}\frac{\partial h\bar{v}}{\partial t} + \frac{\partial h\bar{u}\bar{v}}{\partial x} + \frac{\partial h\bar{v}^2}{\partial y} = {} & -f\bar{u}h - gh\frac{\partial \eta}{\partial y} - \frac{h}{\rho_0}\frac{\partial p_a}{\partial y} - \\ & \frac{gh^2}{2\rho_0}\frac{\partial \rho}{\partial y} + \frac{\tau_{sy}}{\rho_0} - \frac{\tau_{by}}{\rho_0} - \frac{1}{\rho_0}\left(\frac{\partial s_{yx}}{\partial x} + \frac{\partial s_{yy}}{\partial y}\right) + \\ & \frac{\partial}{\partial x}\left(hT_{xy}\right) + \frac{\partial}{\partial y}\left(hT_{yy}\right) + hv_s S\end{aligned} \tag{2.67}$$

The overbar indicates a depth average value. For example, $\bar{u}$ and $\bar{v}$ are the depth-averaged velocities defined by

$$h\bar{u} = \int_{-d}^{\eta} u\,dz\,, \quad h\bar{v} = \int_{-d}^{\eta} v\,dz \tag{2.68}$$

The lateral stresses T_{ij} include viscous friction, turbulent friction and differential advection. They are estimated using an eddy viscosity formulation based on of the depth average velocity gradients

$$T_{xx} = 2A\frac{\partial \bar{u}}{\partial x}, \quad T_{xy} = A\left(\frac{\partial \bar{u}}{\partial y} + \frac{\partial \bar{v}}{\partial x}\right), \quad T_{yy} = 2A\frac{\partial \bar{v}}{\partial y} \tag{2.69}$$

2.3.2 Transport equations for salt and temperature

Integrating the transport equations for salt and temperature over depth the following two-dimensional transport equations are obtained

$$\frac{\partial h\bar{T}}{\partial t} + \frac{\partial h\bar{u}\bar{T}}{\partial x} + \frac{\partial h\bar{v}\bar{T}}{\partial y} = hF_T + h\hat{H} + hT_s S \tag{2.70}$$

$$\frac{\partial h\bar{s}}{\partial t}+\frac{\partial h\bar{u}\bar{s}}{\partial x}+\frac{\partial h\bar{v}\bar{s}}{\partial y}=hF_s+hs_sS \tag{2.71}$$

where $\overline{T}$ and $\bar{s}$ is the depth average temperature and salinity.

2.3.3 Transport equations for a scalar quantity

Integrating the transport equations for a scalar quantity over depth the following two-dimensional transport equations are obtained

$$\frac{\partial h\overline{C}}{\partial t}+\frac{\partial h\bar{u}\overline{C}}{\partial x}+\frac{\partial h\bar{v}\overline{C}}{\partial y}=hF_C-hk_p\overline{C}+hC_sS \tag{2.72}$$

where $\overline{C}$ is the depth average scalar quantity.

2.4 2D Governing Equations in Spherical Coordinates

In spherical coordinates the independent variables are the longitude, λ ,and the latitude, ϕ . The horizontal velocity field (*u*,*v*) is defined by

$$\bar{u}=R\cos\phi\frac{d\lambda}{dt}\qquad\bar{v}=R\frac{d\phi}{dt} \tag{2.73}$$

where *R* is the radius of the earth.

In spherical coordinates the governing equation can be written

$$\frac{\partial h}{\partial t}+\frac{1}{R\cos\phi}\left(\frac{\partial h\bar{u}}{\partial\lambda}+\frac{\partial h\bar{v}\cos\phi}{\partial\phi}\right)=0 \tag{2.74}$$

$$\begin{aligned}&\frac{\partial h\bar{u}}{\partial t}+\frac{1}{R\cos\phi}\left(\frac{\partial h\bar{u}^2}{\partial\lambda}+\frac{\partial h\bar{v}\bar{u}\cos\phi}{\partial\phi}\right)=\left(f+\frac{\bar{u}}{R}\tan\phi\right)\bar{v}h\\&-\frac{1}{R\cos\phi}\left(gh\frac{\partial\eta}{\partial\lambda}-\frac{h}{\rho_0}\frac{\partial p_a}{\partial\lambda}+\frac{gh^2}{2\rho_0}\frac{\partial\rho}{\partial\lambda}+\frac{1}{\rho_0}\left(\frac{\partial s_{xx}}{\partial\lambda}+\cos\phi\frac{\partial s_{xy}}{\partial\phi}\right)\right)+\\&\frac{\tau_{sx}}{\rho_0}-\frac{\tau_{bx}}{\rho_0}+\frac{\partial}{\partial x}\left(hT_{xx}\right)+\frac{\partial}{\partial y}\left(hT_{xy}\right)+hu_sS\end{aligned} \tag{2.75}$$

$$\begin{aligned}&\frac{\partial h\bar{v}}{\partial t}+\frac{1}{R\cos\phi}\left(\frac{\partial h\bar{u}\bar{v}}{\partial\lambda}+\frac{\partial h\bar{v}^2\cos\varphi}{\partial\iota}\right)=-\left(f+\frac{\bar{u}}{R}\tan\phi\right)\bar{u}h\\&-\frac{1}{R}\left(gh\frac{\partial\eta}{\partial\phi}-\frac{h}{\rho_0}\frac{\partial p_a}{\partial\phi}+\frac{gh^2}{2\rho_0}\frac{\partial\rho}{\partial\phi}+\frac{1}{\rho_0}\left(\frac{1}{\cos\phi}\frac{\partial s_{yx}}{\partial\lambda}+\frac{\partial s_{yy}}{\partial\phi}\right)\right)+\\&\frac{\tau_{sy}}{\rho_0}-\frac{\tau_{by}}{\rho_0}+\frac{\partial}{\partial x}\left(hT_{xy}\right)+\frac{\partial}{\partial y}\left(hT_{yy}\right)+hv_sS\end{aligned} \tag{2.76}$$

$$\frac{\partial h\overline{T}}{\partial t}+\frac{1}{R\cos\phi}\left(\frac{\partial h\overline{u}\overline{T}}{\partial\lambda}+\frac{\partial h\overline{v}\overline{T}\cos\phi}{\partial\phi}\right)=hF_T+h\widehat{H}+hT_sS \tag{2.77}$$

$$\frac{\partial h\overline{s}}{\partial t}+\frac{1}{R\cos\phi}\left(\frac{\partial h\overline{u}\overline{s}}{\partial\lambda}+\frac{\partial h\overline{v}\overline{s}\cos\phi}{\partial\phi}\right)=hF_s+hs_sS \tag{2.78}$$

$$\frac{\partial h\overline{C}}{\partial t}+\frac{1}{R\cos\phi}\left(\frac{\partial h\overline{u}\overline{C}}{\partial\lambda}+\frac{\partial h\overline{v}\overline{C}\cos\phi}{\partial\phi}\right)=hF_C-hk_p\overline{C}+hC_sS \tag{2.79}$$

2.5 Bottom Stress

The bottom stress, $\vec{\tau}_b=(\tau_{bx},\tau_{by})$, is determined by a quadratic friction law

$$\frac{\vec{\tau}_b}{\rho_0}=c_f\vec{u}_b|\vec{u}_b| \tag{2.80}$$

where c_f is the drag coefficient and $\vec{u}_b=(u_b,v_b)$ is the flow velocity above the bottom. The friction velocity associated with the bottom stress is given by

$$U_{\tau b}=\sqrt{c_f|u_b|^2} \tag{2.81}$$

For two-dimensional calculations $\vec{u}_b$ is the depth-average velocity and the drag coefficient can be determined from the Chezy number, C, or the Manning number, M

$$c_f=\frac{g}{C^2} \tag{2.82}$$

$$c_f=\frac{g}{\left(Mh^{1/6}\right)^2} \tag{2.83}$$

For three-dimensional calculations $\vec{u}_b$ is the velocity at a distance Δz_b above the sea bed and the drag coefficient is determined by assuming a logarithmic profile between the seabed and a point Δz_b above the seabed

$$c_f=\frac{1}{\left(\frac{1}{\kappa}\ln\left(\frac{\Delta z_b}{z_0}\right)\right)^2} \tag{2.84}$$

where κ=0.4 is the von Kármán constant and z_0 is the bed roughness length scale. When the boundary surface is rough, z_0, depends on the roughness height, k_s

$$z_0=mk_s \tag{2.85}$$

where m is approximately 1/30.

Note, that the Manning number can be estimated from the bed roughness length using the following

$$M = \frac{25.4}{k_s^{1/6}} \tag{2.86}$$

The wave induced bed resistance can be determined from

$$c_f = \left(\frac{u_{fc}}{u_b} \right)^2 \tag{2.87}$$

where U_{fc} is the friction velocity calculated by considering the conditions in the wave boundary layer. For a detailed description of the wave induced bed resistance, see Fredsøe (1984) and Jones et.al. (2014).

2.6 Wind Stress

In areas not covered by ice the surface stress, $\vec{\tau}_s = (\tau_{sx}, \tau_{sy})$, is determined by the winds above the surface. The stress is given by the following empirical relation

$$\bar{\tau}_s = \rho_a c_d |u_w| \bar{u}_w \tag{2.88}$$

where ρ_a is the density of air, c_d is the drag coefficient of air, and $\vec{u}_w = (u_w, v_w)$ is the wind speed 10 m above the sea surface. The friction velocity associated with the surface stress is given by

$$U_{\tau s} = \sqrt{\frac{\rho_a c_f |\bar{u}_w|^2}{\rho_0}} \tag{2.89}$$

The drag coefficient can either be a constant value or depend on the wind speed. The empirical formula proposed by Wu (1980, 1994) is used for the parameterisation of the drag coefficient.

$$c_f = \begin{cases} c_a & w_{10} < w_a \\ c_a + \dfrac{c_b - c_a}{w_b - w_a}\left(w_{10} - w_a\right) & w_a \le w_{10} < w_b \\ c_b & w_{10} \ge w_b \end{cases} \tag{2.90}$$

where c_a, c_b, w_a and w_b are empirical factors and w_{10} is the wind velocity 10 m above the sea surface. The default values for the empirical factors are $c_a = 1.255 \cdot 10^{-3}$, $c_b = 2.425 \cdot 10^{-3}$, $w_a = 7$ m/s and $w_b = 25$ m/s. These give generally good results for open sea applications. Field measurements of the drag coefficient collected over lakes indicate that the drag coefficient is larger than open ocean data. For a detailed description of the drag coefficient see Geernaert and Plant (1990).

2.7 Ice Coverage

It is possible to take into account the effects of ice coverage on the flow field.

In areas where the sea is covered by ice the wind stress is excluded. Instead, the surface stress is caused by the ice roughness. The surface stress, $\vec{\tau}_s = (\tau_{sx}, \tau_{sy})$, is determined by a quadratic friction law

$$\frac{\vec{\tau}_s}{\rho_0} = c_f \vec{u}_s |\vec{u}_s| \tag{2.91}$$

where c_f is the drag coefficient and $\vec{u}_s = (u_s, v_s)$ is the flow velocity below the surface. The friction velocity associated with the surface stress is given by

$$U_{\tau s} = \sqrt{c_f |u_s|^2} \tag{2.92}$$

For two-dimensional calculations $\vec{u}_s$ is the depth-average velocity and the drag coefficient can be determined from the Manning number, M

$$c_f = \frac{g}{\left(Mh^{1/6}\right)^2} \tag{2.93}$$

The Manning number is estimated from the bed roughness length using the following

$$M = \frac{25.4}{k_s^{1/6}} \tag{2.94}$$

For three-dimensional calculations $\vec{u}_s$ is the velocity at a distance Δz_s below the surface and the drag coefficient is determined by assuming a logarithmic profile between the surface and a point Δz_b below the surface

$$c_f = \frac{1}{\left(\frac{1}{\kappa}\ln\left(\frac{\Delta z_s}{z_0}\right)\right)^2} \tag{2.95}$$

where κ=0.4 is the von Kármán constant and z_0 is the bed roughness length scale. When the boundary surface is rough, z_0, depends on the roughness height, k_s

$$z_0 = mk_s \tag{2.96}$$

where m is approximately 1/30.

If ice thickness is specified, the water level is supressed by ρ_{ice} / ρ_{water} of the ice thickness, where ρ_{ice} = 971 kg/m^3 and ρ_{water} is the actual density of the water.

2.8 Tidal Potential

The tidal potential is a force, generated by the variations in gravity due to the relative motion of the earth, the moon and the sun that act throughout the computational domain. The forcing is expanded in frequency space and the potential considered as the sum of a number of terms each representing different tidal constituents. The forcing is implemented as a so-called equilibrium tide, which can be seen as the elevation that theoretically would occur, provided the earth was covered with water. The forcing enters the momentum equations (e.g. (2.66) or (2.75)) as an additional term representing the gradient of the equilibrium tidal elevations, such that the elevation η can be seen as the sum of the actual elevation and the equilibrium tidal potential.

$$\eta = \eta_{ACTUAL} + \eta_T \tag{2.97}$$

The equilibrium tidal potential η_T is given as

$$\eta_T = \sum_i e_i H_i f_i L_i \cos(2\pi \frac{t}{T_i} + b_i + i_0 x) \tag{2.98}$$

where η_T is the equilibrium tidal potential, i refers to constituent number (note that the constituents here are numbered sequentially), e_i is a correction for earth tides based on Love numbers, H_i is the amplitude, f_i is a nodal factor, L_i is given below, t is time, T_i is the period of the constituent, b_i is the phase and x is the longitude of the actual position.

The phase b is based on the motion of the moon and the sun relative to the earth and can be given by

$$b_i = (i_1 - i_0)s + (i_2 + i_0)h + i_3 p + i_4 N + i_5 p_s + u_i \sin(N) \tag{2.99}$$

where i_0 is the species, i_1 to i_5 are Doodson numbers, u is a nodal modulation factor (see Table 2.3) and the astronomical arguments s, h, p, N and p_s are given in Table 2.2.

Table 2.2 Astronomical arguments (Pugh, 1987)

Mean longitude of the moon	s	277.02+481267.89T+0.0011T^2
Mean longitude of the sun	h	280.19+36000.77T+0.0003T^2
Longitude of lunar perigee	p	334.39+4069.04T-0.0103T^2
Longitude of lunar ascending node	N	259.16-1934.14T+0.0021T^2
Longitude of perihelion	p_s	281.22+1.72T+0.0005T^2

In Table 2.2 the time, T, is in Julian century from January 1 1900 UTC, thus T = (365(y – 1900) + (d – 1) + i)/36525 and i = *int* (y-1901)/4), y is year and d is day number

L depends on species number i_0 and latitude y as

$i_0 = 0$ $\quad L = 3\sin^2(y) - 1$

$i_0 = 1$ $\quad L = \sin(2y)$

$i_0 = 2$ $\quad L = \cos^2(y)$

The nodal factor f_i represents modulations to the harmonic analysis and can for some constituents be given as shown in Table 2.3.

Table 2.3 Nodal modulation terms (Pugh, 1987)

	f_i	u_i
M_m	1.000 - 0.130 cos(N)	0
M_f	1.043 + 0.414 cos(N)	-23.7 sin(N)
Q_1, O_1	1.009 + 0.187 cos(N)	10.8 sin(N)
K_1	1.006 + 0.115 cos(N)	-8.9 sin(N)
$2N_2$, μ_2, ν_2, N_2, M_2	1.000 - 0.037 cos(N)	-2.1 sin(N)
K_2	1.024 + 0.286 cos(N)	-17.7 sin(N)

2.9 Wave Radiation

The second order stresses due to breaking of short period waves can be included in the simulation. The radiation stresses act as driving forces for the mean flow and can be used to calculate wave induced flow. For 3D simulations a simple approach is used. Here a uniform variation is used for the vertical variation in radiation stress.

2.10 Heat Exchange

The heat exchange with the atmosphere is calculated on basis of the four physical processes

- Latent heat flux (or the heat loss due to vaporisation)
- Sensible heat flux (or the heat flux due to convection)
- Net short wave radiation
- Net long wave radiation

Latent and sensible heat fluxes and long-wave radiation are assumed to occur at the surface. The absorption profile for the short-wave flux is approximated using Beer's law. The attenuation of the light intensity is described through the modified Beer's law as

$$I(d) = (1-\beta) I_0 e^{-\lambda d} \tag{2.100}$$

where $I(d)$ is the intensity at depth d below the surface; I_0 is the intensity just below the water surface; β is a quantity that takes into account that a fraction of light energy (the infrared) is absorbed near the surface; λ is the light extinction coefficient. Typical values for β and λ are 0.2-0.6 and 0.5-1.4 m^{-1}, respectively. β and λ are user-specified constants. The default values are $\beta = 0.3$ and $\lambda = 1.0\ m^{-1}$. The fraction of the light energy that is absorbed near the surface is βI_0. The net short-wave radiation, $q_{sr,net}$, is attenuated as described by the modified Beer's law. Hence the surface net heat flux is given by

$$Q_n = q_v + q_c + \beta q_{sr,net} + q_{lr,net} \tag{2.101}$$

For three-dimensional calculations the source term $\widehat{H}$ is given by

$$\widehat{H} = \frac{\partial}{\partial z}\left(\frac{q_{sr,net}(1-\beta)e^{-\lambda(\eta-z)}}{\rho_0 c_p}\right) = \frac{q_{sr,net}(1-\beta)\,\lambda e^{-\lambda(\eta-z)}}{\rho_0 c_p} \tag{2.102}$$

For two-dimensional calculations the source term $\widehat{H}$ is given by

$$\widehat{H} = \frac{q_v + q_c + q_{sr,net} + q_{lr,net}}{\rho_0 c_p} \tag{2.103}$$

The calculation of the latent heat flux, sensible heat flux, net short wave radiation, and net long wave radiation as described in the following sections.

In areas covered by ice the heat exchange is excluded.

2.10.1 Vaporisation

Dalton's law yields the following relationship for the vaporative heat loss (or latent flux), see Sahlberg, 1984

$$q_v = LC_e(a_1 + b_1 W_{2m})(Q_{water} - Q_{air}) \tag{2.104}$$

where $L = 2.5 \cdot 10^6\ J/kg$ is the latent heat vaporisation (in the literature $L = 2.5 \cdot 10^6 - 2300\, T_{water}$ is commonly used); $C_e = 1.32 \cdot 10^{-3}$ is the moisture transfer coefficient (or Dalton number); W_{2m} is the wind speed 2 m above the sea surface; Q_{water} is the water vapour density close to the surface; Q_{air} is the water vapour density in the atmosphere; a_1 and b_1 are user specified constants. The default values are $a_1 = 0.5$ and $b_1 = 0.9$.

Measurements of Q_{water} and Q_{air} are not directly available but the vapour density can be related to the vapour pressure as

$$Q_i = \frac{0.2167}{T_i + T_k} e_i \tag{2.105}$$

in which subscript *i* refers to both water and air. The vapour pressure close to the sea, e_{water}, can be expressed in terms of the water temperature assuming that the air close to the surface is saturated and has the same temperature as the water

$$e_{water} = 6.11 e^K \left(\frac{1}{T_k} - \frac{1}{T_{water} + T_k}\right) \tag{2.106}$$

where $K = 5418\,°K$ and $T_K = 273.15\,°K$ is the temperature at 0 C. Similarly the vapour pressure of the air, e_{air}, can be expressed in terms of the air temperature and the relative humidity, R

$$e_{air} = R \cdot 6.11 e^{K\left(\frac{1}{T_k} - \frac{1}{T_{air} + T_k}\right)} \tag{2.107}$$

Replacing Q_{water} and Q_{air} with these expressions the latent heat can be written as

$$q_v = -P_v \left(a_1 + b_1 W_{2m}\right) \cdot \left(\frac{\exp\left(K\left(\frac{1}{T_k} - \frac{1}{T_{water} + T_k}\right)\right)}{T_{water} + T_k} - \frac{R \cdot \exp\left(K\left(\frac{1}{T_k} - \frac{1}{T_{air} + T_k}\right)\right)}{T_{air} + T_k} \right) \tag{2.108}$$

where all constants have been included in a new latent constant $P_v = 4370\ J \cdot °K / m^3$. During cooling of the surface the latent heat loss has a major effect with typical values up to 100 W/m^2.

The wind speed, W_2, 2 m above the sea surface is calculated from the from the wind speed, W_{10}, 10 m above the sea surface using the following formula:

Assuming a logarithmic profile the wind speed, *u(z),* at a distance *z* above the sea surface is given by

$$u(z) = \frac{u_*}{\kappa} \log\left(\frac{z}{z_o}\right) \tag{2.109}$$

where u_* is the wind friction velocity, z_0 is the sea roughness and κ=0.4 is von Karman's constant. u_* and z_0 are given by

$$z_0 = z_{Charnock} u_*^2 / g \tag{2.110}$$

$$u_* = \frac{\kappa u(z)}{\log\left(\frac{z}{z_0}\right)} \tag{2.111}$$

where $z_{Charnock}$ is the Charnock parameter. The default value is $z_{Charnock} = 0.014$. The wind speed, W_2, 2 m above the sea surface is then calculated from the from the wind speed, W_{10}, 10m above the sea surface by first solving Eq. (2.114) and Eq. (2.115) iteratively for z_0 with *z=10m* and *u(z)=*W_{10}. Then W_2 is given by

$$W_2 = W_{10}\frac{\log\left(\frac{2}{z_o}\right)}{\log\left(\frac{10}{z_0}\right)} \qquad W_{10} > 0.5m/s$$
$$W_2 = W_{10} \qquad W_{10} \le 0.5m/s \tag{2.112}$$

The heat loss due to vaporization occurs both by wind driven forced convection by and free convection. The effect of free convection is taken into account by the parameter a_1 in Eq. (2.104). The free convection is also taken into account by introducing a critical wind speed $W_{critical}$ so that the wind speed used in Eq. (2.112) is obtained as $W_{10}=max(W_{10},W_{critical})$. The default value for the critical wind speed is 2 m/s.

2.10.2 Convection

The sensible heat flux, q_c (W/m^2) , (or the heat flux due to convection) depends on the type of boundary layer between the sea surface and the atmosphere. Generally this boundary layer is turbulent implying the following relationship

$$q_c = \begin{cases} \rho_{air} c_{air} c_{heating} W_{10}(T_{air} - T_{water}) & T_{air} \ge T \\ \rho_{air} c_{air} c_{cooling} W_{10}(T_{air} - T_{water}) & T_{air} < T \end{cases} \tag{2.113}$$

where ρ_{air} is the air density 1.225 kg/m^3; $c_{air} = 1007\ J/(kg\cdot°K)$ is the specific heat of air; $c_{heating} = 0.0011$ and $c_{cooling} = 0.0011$, respectively, is the sensible transfer coefficient (or Stanton number) for heating and cooling (see Kantha and Clayson, 2000); W_{10} is the wind speed 10 m above the sea surface; T_{water} is the temperature at the sea surface; T_{air} is the temperature of the air.

The convective heat flux typically varies between 0 and 100 W/m^2.

The heat loss due to convection occurs both by wind driven forced convection by and free convection. The free convection is taken into account by introducing a critical wind speed $W_{critical}$ so that the wind speed used in Eq. (2.113) is obtained as $W_{10}=max(W_{10},W_{critical})$. The default value for the critical wind speed is 2 m/s.

2.10.3 Short wave radiation

Radiation from the sun consists of electromagnetic waves with wave lengths varying from 1,000 to 30,000 Å. Most of this is absorbed in the ozone layer, leaving only a fraction of the energy to reach the surface of the Earth. Furthermore, the spectrum changes when sunrays pass through the atmosphere. Most of the infrared and ultraviolet compound is absorbed such that the solar radiation on the Earth mainly consists of light with wave lengths between 4,000 and 9,000 Å. This radiation is normally termed short wave radiation. The intensity depends on the distance to the sun, declination angle and latitude, extraterrestrial radiation and the cloudiness and amount of water vapour in the atmosphere (see Iqbal, 1983)

The eccentricity in the solar orbit, E_0, is given by

$$E_0 = \left(\frac{r_0}{r}\right)^2 = 1.000110 + 0.034221\cos(\Gamma) + 0.001280\sin(\Gamma) + 0.000719\cos(2\Gamma) + 0.000077\sin(2\Gamma) \quad (2.114)$$

where r_0 is the mean distance to the sun, r is the actual distance and the day angle $\Gamma\ (rad)$ is defined by

$$\Gamma = \frac{2\pi(d_n - 1)}{365} \quad (2.115)$$

and d_n is the Julian day of the year.

The daily rotation of the Earth around the polar axes contributes to changes in the solar radiation. The seasonal radiation is governed by the declination angle, $\delta\ (rad)$, which can be expressed by

$$\delta = 0.006918 - 0.399912\cos(\Gamma) + 0.07257\sin(\Gamma) - 0.006758\cos(2\Gamma) + 0.000907\sin(2\Gamma) - 0.002697\cos(3\Gamma) + 0.00148\sin(3\Gamma) \quad (2.116)$$

The day length, n_d, varies with δ. For a given latitude, ϕ, (positive on the northern hemisphere) the day length is given by

$$n_d = \frac{24}{\pi}\arccos\left(-\tan(\phi)\tan(\delta)\right) \quad (2.117)$$

and the sunrise angle, $\omega_{sr}\ (rad)$, and the sunset angle $\omega_{ss}\ (rad)$ are

$$\omega_{sr} = \arccos\left(-\tan(\phi)\tan(\delta)\right) \quad and \quad \omega_{ss} = -\omega_{sr} \quad (2.118)$$

The intensity of short wave radiation on the surface parallel to the surface of the Earth changes with the angle of incidence. The highest intensity is in zenith and the lowest during sunrise and sunset. Integrated over one day the extraterrestrial intensity, $H_0\ (MJ/m^2/day)$, in short wave radiation on the surface can be derived as

$$H_0 = \frac{24}{\pi} q_{sc} E_0 \cos(\phi)\cos(\delta)\left(\sin(\omega_{sr}) - \omega_{sr}\cos(\omega_{sr})\right) \quad (2.119)$$

where $q_{sc} = 4.9212\ (MJ/m^2/h)$ is the solar constant.

For determination of daily radiation under cloudy skies, $H\ (MJ/m^2/day)$, the following relation is used

$$\frac{H}{H_0} = a_2 + b_2 \frac{n}{n_d} \tag{2.120}$$

in which n is the number of sunshine hours and n_d is the maximum number of sunshine hours. a_2 and b_2 are user specified constants. The default values are $a_2 = 0.295$ and $b_2 = 0.371$. The user-specified clearness coefficient corresponds to n/n_d. Thus the solar radiation, q_s (W/m^2), can be expressed as

$$q_s = \left(\frac{H}{H_0}\right) q_0 \left(a_3 + b_3 \cos(\omega_i)\right) \frac{10^6}{3600} \tag{2.121}$$

where

$$a_3 = 0.4090 + 0.5016 \sin\left(\omega_{sr} - \frac{\pi}{3}\right) \tag{2.122}$$

$$b_3 = 0.6609 + 0.4767 \sin\left(\omega_{sr} - \frac{\pi}{3}\right) \tag{2.123}$$

The extraterrestrial intensity, q_0 $(MJ/m^2/h)$ and the hour angle ω_i is given by

$$q_0 = q_{sc} E_0 \left(\sin(\phi)\sin(\delta) + \frac{24}{\pi}\cos(\phi)\cos(\delta)\cos(\omega_i)\right) \tag{2.124}$$

$$\omega_i = \frac{\pi}{12}\left(12 + \Delta t_{displacement} + \frac{4}{60}(L_S - L_E) - \frac{E_t}{60} - t_{local}\right) \tag{2.125}$$

$\Delta t_{displacement}$ is the displacement hours due to summer time and the time meridian L_S is the standard longitude for the time zone. $\Delta t_{displacement}$ and L_S are user specified constants. The default values are $\Delta t_{displacement} = 0$ (h) and $L_S = 0$ $(\deg)$. L_E is the local longitude in degrees. E_t (s) is the discrepancy in time due to solar orbit and is varying during the year. It is given by

$$E_t = \begin{pmatrix} 0.000075 + 0.001868\cos(\Gamma) - 0.032077\sin(\Gamma) \\ -0.014615\cos(2\Gamma) - 0.04089\sin(2\Gamma) \end{pmatrix} \cdot 229.18 \tag{2.126}$$

Finally, t_{local} is the local time in hours.

Solar radiation that impinges on the sea surface does not all penetrate the water surface. Parts are reflected back and are lost unless they are backscattered from the surrounding atmosphere. This reflection of solar energy is termed the albedo. The amount of energy, which is lost due to albedo, depends on the angle of incidence and angle of refraction. For a smooth sea the reflection can be expressed as

$$\alpha = \frac{1}{2}\left(\frac{\sin^2(i-r)}{\sin^2(i+r)} + \frac{\tan^2(i-r)}{\tan^2(i+r)}\right) \tag{2.127}$$

where *i* is the angle of incidence, *r* the refraction angle and α the reflection coefficient, which typically varies from 5 to 40 %. α can be approximated using

$$\alpha = \begin{cases} \frac{altitude}{5}\,0.48 & altitude < 5 \\ \frac{30 - altitude}{25}(0.48 - 0.05) & 5 \le altitude \le 30 \\ 0.05 & altitude > 30 \end{cases} \tag{2.128}$$

where the altitude in degrees is given by

$$altitude = 90 - \left(\frac{180}{\pi}\arccos(\sin(\delta)\sin(\phi) + \cos(\delta)\cos(\phi)\cos(\omega_i))\right) \tag{2.129}$$

Thus the net short wave radiation, $q_{s,net}$ (W/m^2), can possibly be expressed as

$$q_{sr,net} = (1-\alpha)q_s \tag{2.130}$$

The net short wave radiation, $q_{sr,net}$, can be calculated using empirical formulae as described above. Alternatively, the net short wave radiation can be calculated using Eq. (2.130) where the solar radiation, q_s, is specified by the user or the net short wave radiation, $q_{sr,net}$, can be given by the user.

2.10.4 Long wave radiation

A body or a surface emits electromagnetic energy at all wavelengths of the spectrum. The long wave radiation consists of waves with wavelengths between 9,000 and 25,000 Å. The radiation in this interval is termed infrared radiation and is emitted from the atmosphere and the sea surface. The long wave emittance from the surface to the atmosphere minus the long wave radiation from the atmosphere to the sea surface is called the net long wave radiation and is dependent on the cloudiness, the air temperature, the vapour pressure in the air and the relative humidity. The net outgoing long wave radiation, $q_{lr,net}$ (W/m^2), is given by Brunt's equation (See Lind and Falkenmark, 1972)

$$q_{lr,net} = -\sigma_{sb}(T_{air} + T_K)^4\left(a - b\sqrt{e_d}\right)\left(c + d\,\frac{n}{n_d}\right) \tag{2.131}$$

where e_d is the vapour pressure at dew point temperature measured in *mb*; n is the number of sunshine hours, n_d is the maximum number of sunshine hours; $\sigma_{sb} = 5.6697 \cdot 10^{-8}\ W/(m^2 \cdot °K^4)$ is Stefan Boltzman's constant; $T_{air}\,(°C)$ is the air temperature. The coefficients *a*, *b*, *c* and *d* are given as

$$a = 0.56; b = 0.077 mb^{-½}; c = 0.10; d = .90 \quad (2.132)$$

The vapour pressure is determined as

$$e_d = 10 \cdot R\, e_{saturated} \quad (2.133)$$

where *R* is the relative humidity and the saturated vapour pressure, $e_{saturated}\,(kPa)$, with 100 % relative humidity in the interval from –51 to 52 °C can be estimated by

$$e_{saturated} = 3.38639 \cdot \left(\left(7.38 \cdot 10^{-3} \cdot T_{air} + 0.8072\right)^8 - 1.9 \cdot 10^{-5} \left|1.8 \cdot T_{air} + 48\right| + 1.316 \cdot 10^{-3}\right) \quad (2.134)$$

The net long wave radiation, $q_{lr,net}$, can be calculated using empirical formulae as described above. Alternatively, the net long wave radiation can be calculated as

$$q_{lr,net} = q_{ar,net} - q_{br} \quad (2.135)$$

where the net incident atmospheric radiation, $q_{ar,net}$, is specified by the user and the back radiation, q_{br}, is given by

$$q_{br} = (1 - r)\varepsilon\sigma_{sb} T_K^4 \quad (2.136)$$

where r=0.03 is the reflection coefficient and ε=0.985 is the emissivity factor of the atmosphere. The net long wave radiation can also be specified by the user.

3 Numerical Solution

3.1 Spatial Discretization

The discretization in solution domain is performed using a finite volume method. The spatial domain is discretized by subdivision of the continuum into non-overlapping cells/elements.

In the two-dimensional case the elements can be arbitrarily shaped polygons, however, here only triangles and quadrilateral elements are considered.

In the three-dimensional case a layered mesh is used: in the horizontal domain an unstructured mesh is used while in the vertical domain a structured mesh is used (see Figure 3.1). The vertical mesh is based on either sigma coordinates or combined sigma/z-level coordinates. For the hybrid sigma/z-level mesh sigma coordinates are used from the free surface to a specified depth and z-level coordinates are used below. The different types of vertical mesh are illustrated in Figure 3.2. The elements in the sigma domain and the z-level domain can be prisms with either a 3-sided or 4-sided polygonal base. Hence, the horizontal faces are either triangles or quadrilateral element. The elements are perfectly vertical and all layers have identical topology.

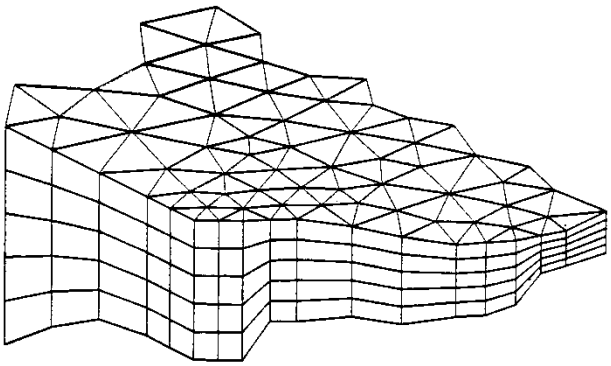

Figure 3.1 Principle of meshing for the three-dimensional case

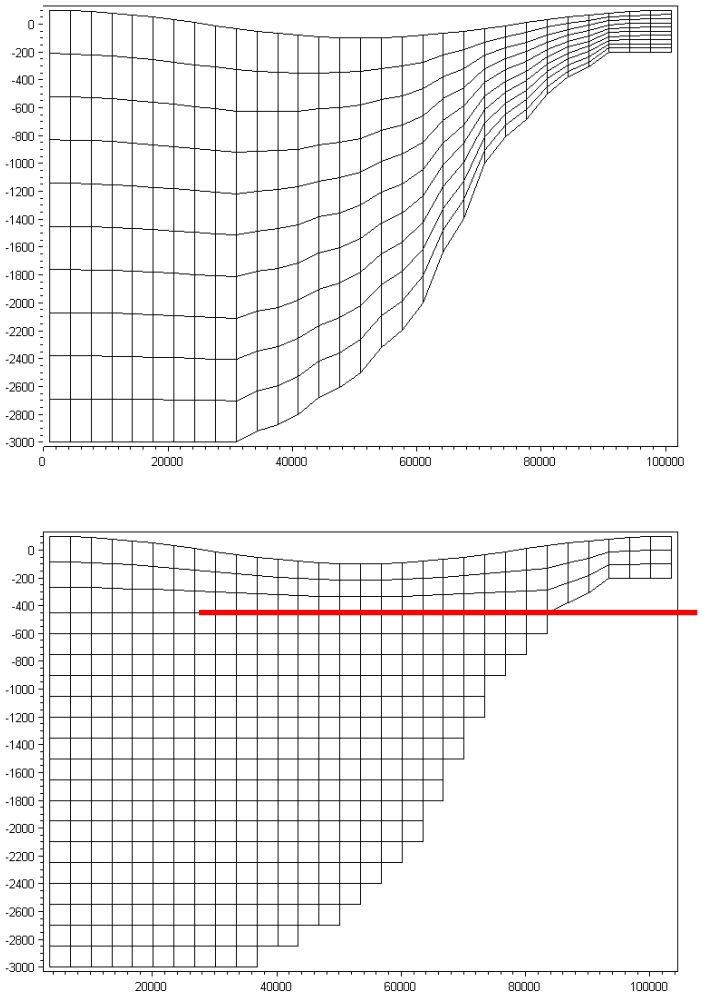

Figure 3.2 Illustrations of the different vertical grids. Upper: sigma mesh, Lower: combined sigma/z-level mesh with simple bathymetry adjustment. The red line shows the interface between the z-level domain and the sigma-level domain

The most important advantage using sigma coordinates is their ability to accurately represent the bathymetry and provide consistent resolution near the bed. However, sigma coordinates can suffer from significant errors in the horizontal pressure gradients, advection and mixing terms in areas with sharp topographic changes (steep slopes). These errors can give rise to unrealistic flows.

The use of z-level coordinates allows a simple calculation of the horizontal pressure gradients, advection and mixing terms, but the disadvantages are their inaccuracy in representing the bathymetry and that the stair-step representation of the bathymetry can result in unrealistic flow velocities near the bottom.

3.1.1 Vertical Mesh

For the vertical discretization both a standard sigma mesh and a combined sigma/z-level mesh can be used. For the hybrid sigma/z-level mesh sigma coordinates are used from the free surface to a specified depth, z_σ, and z-level coordinates are used below. At least one sigma layer is needed to allow changes in the surface elevation.

Sigma

In the sigma domain a constant number of layers, N_σ, are used and each sigma layer is a fixed fraction of the total depth of the sigma layer, h_σ, where $h_\sigma = \eta - \max(z_b, z_\sigma)$. The discretization in the sigma domain is given by a number of discrete σ-levels $\{\sigma_i,\ \ i = 1, (N_\sigma + 1)\}$. Here σ varies from $\sigma_1 = 0$ at the bottom interface of the lowest sigma layer to $\sigma_{N_\sigma+1} = 1$ at the free surface.

Variable sigma coordinates can be obtained using a discrete formulation of the general vertical coordinate (s-coordinate) system proposed by Song and Haidvogel (1994). First an equidistant discretization in a s-coordinate system *(-1≤ s ≤0*) is defined

$$s_i = -\frac{N_\sigma + 1 - i}{N_\sigma} \qquad i = 1, (N_\sigma + 1) \tag{3.1}$$

The discrete sigma coordinates can then be determined by

$$\sigma_i = 1 + \sigma_c s_i + (1 - \sigma_c) c(s_i) \quad i = 1, (N_\sigma + 1) \tag{3.2}$$

where

$$c(s) = (1 - b)\frac{\sinh(\theta s)}{\sinh(\theta)} + b\frac{\tanh\left(\theta\left(s + \frac{1}{2}\right)\right) - \tanh(\frac{\theta}{2})}{2\tanh(\frac{\theta}{2})} \tag{3.3}$$

Here σ_c is a weighting factor between the equidistant distribution and the stretch distribution, θ is the surface control parameter and b is the bottom control parameter. The range for the weighting factor is $0<\sigma_c\leq 1$ where the value 1 corresponds to equidistant distribution and 0 corresponds to stretched distribution. A small value of σ_c can result in linear instability. The range of the surface control parameter is $0<\theta\leq 20$ and the range of the bottom control parameter is $0\leq b\leq 1$. If $\theta<<1$ and $b=0$ an equidistant vertical resolution is obtained. By increasing the value of the θ, the highest resolution is achieved near the surface. If $\theta>0$ and $b=1$ a high resolution is obtained both near the surface and near the bottom.

Examples of a mesh using variable vertical discretization are shown in Figure 3.3 and Figure 3.4.

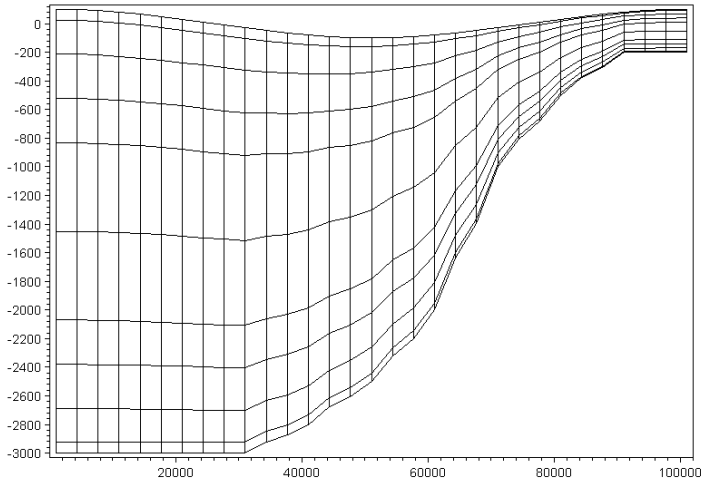

Figure 3.3 Example of vertical distribution using layer thickness distribution. Number of layers: 10, thickness of layers 1 to 10: .025, 0.075, 0.1, 0.01, 0.02, 0.02, 0.1, 0.1, 0.075, 0.025

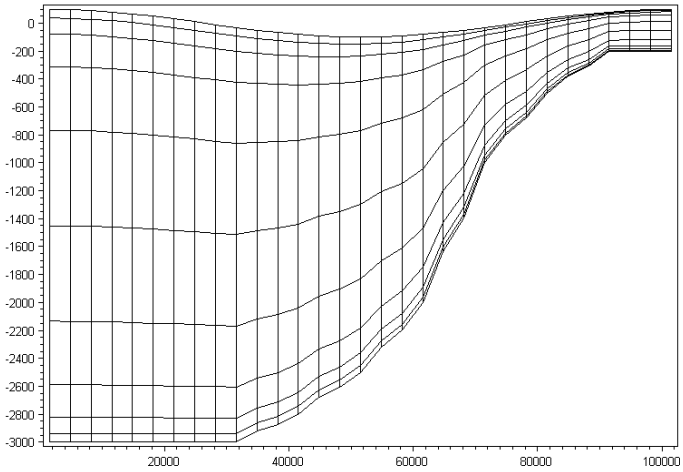

Figure 3.4 Example of vertical distribution using variable distribution. Number of layers: 10, σ_c = 0.1, θ = 5, b = 1

Combined sigma/z-level

In the z-level domain the discretization is given by a number of discrete z-levels $\{z_i,\ i = 1, (N_z + 1)\}$, where N_z is the number of layers in the z-level domain. z_1 is the minimum z-level and z_{N_z+1} is the maximum z-level, which is equal to the sigma depth, z_σ. The corresponding layer thickness is given by

$$\Delta z_i = z_{i+1} - z_i \qquad i = 1, N_z \tag{3.4}$$

The discretization is illustrated in Figure 3.5 and Figure 3.6.

Using standard z-level discretization the bottom depth is rounded to the nearest z-level. Hence, for a cell in the horizontal mesh with the cell-averaged depth, z_b, the cells in the corresponding column in the z-domain are included if the following criteria is satisfied

$$(\mathrm{z_{i+1}} - \mathrm{z_i})/2 \geq z_b \quad i = 1, N_z \tag{3.5}$$

The cell-averaged depth, z_b, is calculated as the mean value of the depth at the vortices of each cell. For the standard z-level discretization the minimum depth is given by z_1. Too take into account the correct depth for the case where the bottom depth is below the minimum z-level ($z_1 > z_b$) a bottom fitted approach is used. Here, a correction factor, f_1, for the layer thickness in the bottom cell is introduced. The correction factor is used in the calculation of the volume and face integrals. The correction factor for the bottom cell is calculated by

$$f_1 = \frac{(z_2 - z_b)}{\Delta z_1} \tag{3.6}$$

The corrected layer thickness is given by $\Delta z_1^* = f_1 \Delta z_1$. The simple bathymetry adjustment approach is illustrated in Figure 3.5.

For a more accurate representation of the bottom depth an advanced bathymetry adjustment approach can be used. For a cell in the horizontal mesh with the cell-averaged depth, z_b, the cells in the corresponding column in the z-domain are included if the following criteria is satisfied

$$z_{i+1} > z_b \qquad i = 1, N_z \tag{3.7}$$

A correction factor, f_i, is introduced for the layer thickness

$$f_i = max\left(\frac{(z_{i+1} - z_b)}{\Delta z_i}, \frac{z_{min}}{\Delta z_i}\right) \qquad z_i < z_b < z_{i+1} \;\; or \;\; z_1 > z_b$$
$$f_i = 1 \qquad z_1 \geq z_b \tag{3.8}$$

A minimum layer thickness, Δz_{min}, is introduced to avoid very small values of the correction factor. The correction factor is used in the calculation of the volume and face integrals. The corrected layer thicknesses are given by $\{\Delta z_i^* = f_i \Delta z_i, \; i = 1, N_z\}$. The advanced bathymetry adjustment approach is illustrated in Figure 3.6.

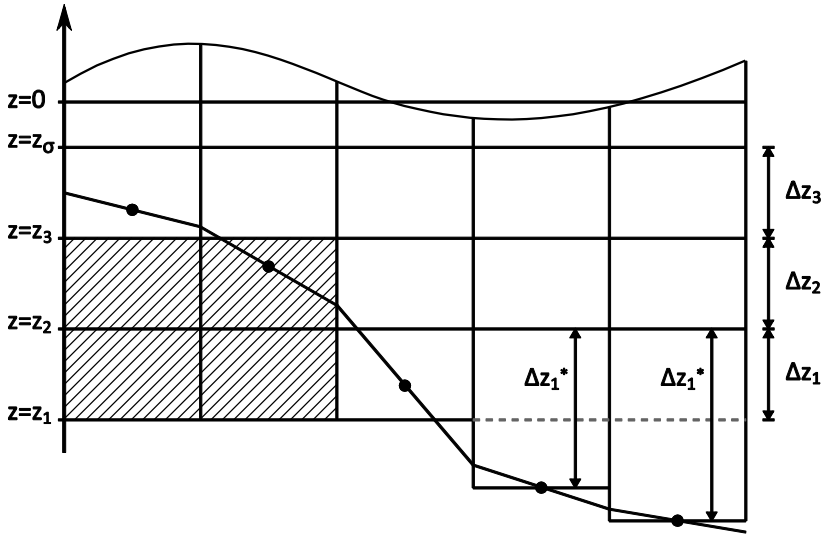

Figure 3.5 Simple bathymetry adjustment approach

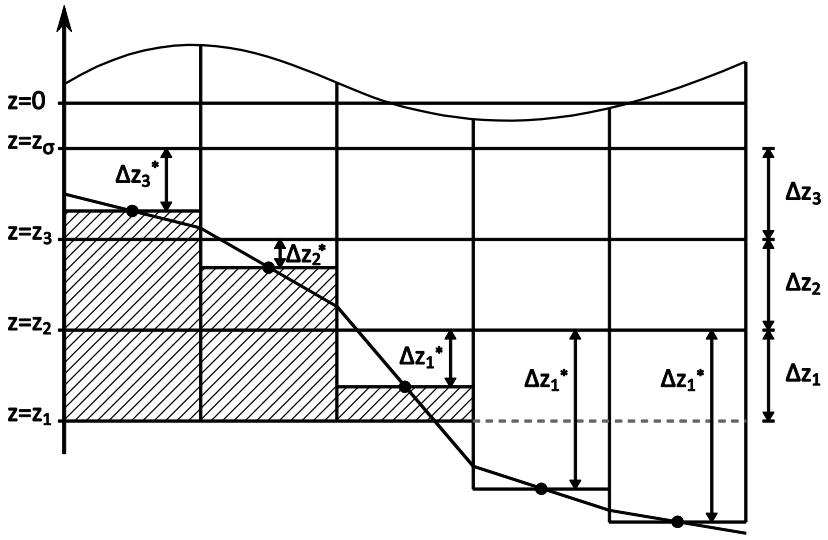

Figure 3.6 Advanced bathymetry adjustment approach

3.1.2 Shallow water equations

The integral form of the system of shallow water equations can in general form be written

$$\frac{\partial \boldsymbol{U}}{\partial t} + \nabla \cdot \boldsymbol{F}(\boldsymbol{U}) = \boldsymbol{S}(\boldsymbol{U}) \tag{3.9}$$

where ***U*** is the vector of conserved variables, ***F*** is the flux vector function and ***S*** is the vector of source terms.

In Cartesian coordinates the system of 2D shallow water equations can be written

$$\frac{\partial \boldsymbol{U}}{\partial t} + \frac{\partial \left(\boldsymbol{F}_x^I - \boldsymbol{F}_x^V \right)}{\partial x} + \frac{\partial \left(\boldsymbol{F}_y^I - \boldsymbol{F}_y^V \right)}{\partial y} = \boldsymbol{S} \tag{3.10}$$

where the superscripts *I* and *V* denote the inviscid (convective) and viscous fluxes, respectively and where

$$\boldsymbol{U} = \begin{bmatrix} h \\ h\bar{u} \\ h\bar{v} \end{bmatrix},$$

$$\boldsymbol{F}_x^{\,I} = \begin{bmatrix} h\bar{u} \\ h\bar{u}^2 + \frac{1}{2}g(h^2 - d^2) \\ h\bar{u}\bar{v} \end{bmatrix}, \quad \mathrm{F}_x^{\,V} = \begin{bmatrix} 0 \\ hA\left(2\frac{\partial \bar{u}}{\partial x}\right) \\ hA\left(\frac{\partial \bar{u}}{\partial y} + \frac{\partial \bar{v}}{\partial x}\right) \end{bmatrix}$$

$$\boldsymbol{F}_y^{\,I} = \begin{bmatrix} h\bar{v} \\ h\bar{v}\bar{u} \\ h\bar{v}^2 + \frac{1}{2}g(h^2 - d^2) \end{bmatrix}_a, \quad \mathrm{F}_y^{\,V} = \begin{bmatrix} 0 \\ hA\left(\frac{\partial \bar{u}}{\partial y} + \frac{\partial \bar{v}}{\partial x}\right) \\ hA\left(2\frac{\partial \bar{v}}{\partial x}\right) \end{bmatrix} \tag{3.11}$$

$$\boldsymbol{S} = \begin{bmatrix} 0 \\ g\eta\frac{\partial d}{\partial x} + f\bar{v}h - \frac{h}{\rho_0}\frac{\partial p_a}{\partial x} - \frac{gh^2}{2\rho_0}\frac{\partial \rho}{\partial x} - \frac{1}{\rho_0}\left(\frac{\partial s_{xx}}{\partial x} + \frac{\partial s_{xy}}{\partial y}\right) \\ \qquad + \frac{\tau_{sx}}{\rho_0} - \frac{\tau_{bx}}{\rho_0} + hu_s \\ g\eta\frac{\partial d}{\partial y} - f\bar{u}h - \frac{h}{\rho_0}\frac{\partial p_a}{\partial y} - \frac{gh^2}{2\rho_0}\frac{\partial \rho}{\partial y} - \frac{1}{\rho_0}\left(\frac{\partial s_{yx}}{\partial x} + \frac{\partial s_{yy}}{\partial y}\right) \\ \qquad + \frac{\tau_{sy}}{\rho_0} - \frac{\tau_{by}}{\rho_0} + hv_s \end{bmatrix}$$

In Cartesian coordinates the system of 3D shallow water equations can be written

$$\frac{\partial \boldsymbol{U}}{\partial t} + \frac{\partial \boldsymbol{F}_x^{\,I}}{\partial x'} + \frac{\partial \boldsymbol{F}_y^{\,I}}{\partial y'} + \frac{\partial \boldsymbol{F}_\sigma^{\,I}}{\partial \sigma} + \frac{\partial \boldsymbol{F}_x^{\,V}}{\partial x} + \frac{\partial \boldsymbol{F}_y^{\,V}}{\partial y} + \frac{\partial \boldsymbol{F}_\sigma^{\,V}}{\partial \sigma} = \boldsymbol{S} \tag{3.12}$$

where the superscripts *I* and *V* denote the inviscid (convective) and viscous fluxes, respectively and where

$$\boldsymbol{U} = \begin{bmatrix} h \\ hu \\ hv \end{bmatrix},$$

$$\boldsymbol{F}_x^{\,I} = \begin{bmatrix} h\bar{u} \\ hu^2 + \frac{1}{2}g(h^2 - d^2) \\ huv \end{bmatrix}, \quad \boldsymbol{F}_x^{\,V} = \begin{bmatrix} 0 \\ hA\left(2\frac{\partial u}{\partial x}\right) \\ hA\left(\frac{\partial u}{\partial y} + \frac{\partial v}{\partial x}\right) \end{bmatrix}$$

$$\boldsymbol{F}_y^{\,I} = \begin{bmatrix} h\bar{v} \\ hvu \\ hv^2 + \frac{1}{2}g(h^2 - d^2) \end{bmatrix}, \quad \boldsymbol{F}_y^{\,V} = \begin{bmatrix} 0 \\ hA\left(\frac{\partial u}{\partial y} + \frac{\partial v}{\partial x}\right) \\ hA\left(2\frac{\partial v}{\partial x}\right) \end{bmatrix} \tag{3.13}$$

$$\boldsymbol{F}_\sigma^{\,I} = \begin{bmatrix} h\omega \\ h\omega u \\ h\omega v \end{bmatrix}, \quad \boldsymbol{F}_\sigma^{\,V} = \begin{bmatrix} 0 \\ \frac{\upsilon_t}{h}\frac{\partial u}{\partial \sigma} \\ \frac{\upsilon_t}{h}\frac{\partial v}{\partial \sigma} \end{bmatrix}$$

$$\boldsymbol{S} = \begin{bmatrix} 0 \\ g\eta\frac{\partial d}{\partial x} + fvh - \frac{h}{\rho_0}\frac{\partial p_a}{\partial x'} - \frac{hg}{\rho_0}\int_z^\eta \frac{\partial \rho}{\partial x}dz - \frac{1}{\rho_0}\left(\frac{\partial s_{xx}}{\partial x} + \frac{\partial s_{xy}}{\partial y}\right) + hu_s \\ g\eta\frac{\partial d}{\partial y} - fuh - \frac{h}{\rho_0}\frac{\partial p_a}{\partial y'} - \frac{hg}{\rho_0}\int_z^\eta \frac{\partial \rho}{\partial y}dz - \frac{1}{\rho_0}\left(\frac{\partial s_{yx}}{\partial x} + \frac{\partial s_{yy}}{\partial y}\right) + hv_s \end{bmatrix}$$

Integrating Eq. (3.9) over the *i*th cell and using Gauss's theorem to rewrite the flux integral gives

$$\int_{A_i} \frac{\partial \boldsymbol{U}}{\partial t} d\Omega + \int_{\Gamma_i} (\boldsymbol{F} \cdot \boldsymbol{n})\, ds = \int_{A_i} \boldsymbol{S}(\boldsymbol{U}) d\Omega \tag{3.14}$$

where A_i is the area/volume of the cell Ω is the integration variable defined on A_i, Γ_i is the boundary of the *i*th cell and *ds* is the integration variable along the boundary. ***n*** is the unit outward normal vector along the boundary. Evaluating the area/volume integrals by a one-point quadrature rule, the quadrature point being the centroid of the cell, and evaluating the boundary intergral using a mid-point quadrature rule, Eq. (3.14) can be written

$$\frac{\partial U_i}{\partial t} + \frac{1}{A_i}\sum_j^{NS} \boldsymbol{F}\cdot\boldsymbol{n}\,\Delta\Gamma_j = S_i \tag{3.15}$$

Here U_i and S_i, respectively, are average values of U and S over the *i*th cell and stored at the cell centre, NS is the number of sides of the cell, n_j is the unit outward normal vector at the *j*th side and $\Delta\Gamma_j$ the length/area of the *j*th interface.

Both a first order and a second order scheme can be applied for the spatial discretization.

For the 2D case an approximate Riemann solver (Roe's scheme, see Roe, 1981) is used to calculate the convective fluxes at the interface of the cells. Using the Roe's scheme the dependent variables to the left and to the right of an interface have to be estimated. Second-order spatial accuracy is achieved by employing a linear gradient-reconstruction technique. The average gradients are estimated using the approach by Jawahar and Kamath, 2000. To avoid numerical oscillations a second order TVD slope limiter (Van Leer limiter, see Hirch, 1990 and Darwish, 2003) is used.

For the 3D case an approximate Riemann solver (Roe's scheme, see Roe, 1981) is used to calculate the convective fluxes at the vertical interface of the cells (x'y'-plane). Using the Roe's scheme the dependent variables to the left and to the right of an interface have to be estimated. Second-order spatial accuracy is achieved by employing a linear gradient-reconstruction technique. The average gradients are estimated using the approach by Jawahar and Kamath, 2000. To avoid numerical oscillations a second order TVD slope limiter (Van Leer limiter, see Hirch, 1990 and Darwish, 2003) is used. The convective fluxes at the horizontal interfaces (vertical line) are derived using first order upwinding for the low order scheme. For the higher order scheme the fluxes are approximated by the mean value of the fluxes calculated based on the cell values above and below the interface for the higher order scheme.

3.1.3 Transport equations

The transport equations arise in the salt and temperature model, the turbulence model and the generic transport model. They all share the form of Equation Eq. (2.20) in Cartesian coordinates. For the 2D case the integral form of the transport equation can be given by Eq. (3.9) where

$$\boldsymbol{U} = h\bar{C}$$

$$\boldsymbol{F}^I = \left[h\bar{u}\bar{C},\quad h\bar{v}\bar{C}\right]$$
$$\boldsymbol{F}^V = \left[hD_h\frac{\partial\bar{C}}{\partial x},\quad hD_h\frac{\partial\bar{C}}{\partial y}\right] \tag{3.16}$$

$$\boldsymbol{S} = -hk_p\bar{C} + hC_sS.$$

For the 3D case the integral form of the transport equation can be given by Eq. (3.9) where

$$\boldsymbol{U} = hC$$

$$\boldsymbol{F}^I = \left[huC, \quad hvC, \quad h\omega C\right]$$
$$\boldsymbol{F}^V = \left[hD_h\partial\frac{\partial C}{\partial x}, \quad hD_h\partial\frac{\partial C}{\partial y}, \quad h\frac{D_h}{h}\partial\frac{\partial C}{\partial \sigma}\right] \tag{3.17}$$

$$\boldsymbol{S} = -hk_pC + hC_sS.$$

The discrete finite volume form of the transport equation is given by Eq. (3.15). As for the shallow water equations both a first order and a second order scheme can be applied for the spatial discretization.

In 2D the low order approximation uses simple first order upwinding, i.e., element average values in the upwinding direction are used as values at the boundaries. The higher order version approximates gradients to obtain second order accurate values at the boundaries. Values in the upwinding direction are used. To provide stability and minimize oscillatory effects, a TVD-MUSCL limiter is applied (see Hirch, 1990, and Darwish, 2003).

In 3D the low order version uses simple first order upwinding. The higher order version approximates horizontal gradients to obtain second order accurate values at the horizontal boundaries. Values in the upwinding direction are used. To provide stability and minimize oscillatory effects, an ENO (Essentially Non-Oscillatory) type procedure is applied to limit the horizontal gradients. In the vertical direction a 3rd order ENO procedure is used to obtain the vertical face values (Shu, 1997).

3.2 Time Integration

Consider the general form of the equations

$$\frac{\partial \boldsymbol{U}}{\partial t} = \boldsymbol{G}\left(\boldsymbol{U}\right) \tag{3.18}$$

For 2D simulations, there are two methods of time integration for both the shallow water equations and the transport equations: A low order method and a higher order method. The low order method is a first order explicit Euler method

$$\boldsymbol{U}_{n+1} = \boldsymbol{U}_n + \Delta t\ \boldsymbol{G}(\boldsymbol{U}_n) \tag{3.19}$$

where Δt is the time step interval. The higher order method uses a second order Runge Kutta method on the form:

$$\boldsymbol{U}_{n+\frac{1}{2}} = \boldsymbol{U}_n + \tfrac{1}{2}\Delta t\ \boldsymbol{G}(\boldsymbol{U}_n)$$
$$\boldsymbol{U}_{n+1} = \boldsymbol{U}_n + \Delta t\ \boldsymbol{G}(\boldsymbol{U}_{n+\frac{1}{2}}) \tag{3.20}$$

For 3D simulations the time integration is semi-implicit. The horizontal terms are treated implicitly and the vertical terms are treated implicitly or partly explicitly and partly implicitly. Consider the equations in the general semi-implicit form.

$$\frac{\partial \boldsymbol{U}}{\partial t} = \boldsymbol{G}_h(\boldsymbol{U}) + \boldsymbol{G}_v(B\boldsymbol{U}) = \boldsymbol{G}_h(\boldsymbol{U}) + \boldsymbol{G}_v^I(\boldsymbol{U}) + \boldsymbol{G}_v^V(\boldsymbol{U}) \tag{3.21}$$

where the h and v subscripts refer to horizontal and vertical terms, respectively, and the superscripts refer to invicid and viscous terms, respectively. As for 2D simulations, there is a lower order and a higher order time integration method.

The low order method used for the 3D shallow water equations can written as

$$\boldsymbol{U}_{n+1} - \tfrac{1}{2}\Delta t\left(\boldsymbol{G}_v(\boldsymbol{U}_{n+1}) + \boldsymbol{G}_v(\boldsymbol{U}_n)\right) = \boldsymbol{U}_n + \Delta t\ \boldsymbol{G}_h(\boldsymbol{U}_n) \tag{3.22}$$

The horizontal terms are integrated using a first order explicit Euler method and the vertical terms using a second order implicit trapezoidal rule. The higher order method can be written

$$\begin{aligned} \boldsymbol{U}_{n+1/2} - \tfrac{1}{4}\Delta t\ \left(\boldsymbol{G}_v(\boldsymbol{U}_{n+1/2}) + \boldsymbol{G}_v(\boldsymbol{U}_n)\right) &= \boldsymbol{U}_n + \tfrac{1}{2}\Delta t\ \boldsymbol{G}_h(\boldsymbol{U}_n) \\ \boldsymbol{U}_{n+1} - \tfrac{1}{2}\Delta t\ \left(\boldsymbol{G}_v(\boldsymbol{U}_{n+1}) + \boldsymbol{G}_v(\boldsymbol{U}_n)\right) &= \boldsymbol{U}_n + \Delta t\ \boldsymbol{G}_h(\boldsymbol{U}_{n+1/2}) \end{aligned} \tag{3.23}$$

The horizontal terms are integrated using a second order Runge Kutta method and the vertical terms using a second order implicit trapezoidal rule.

The low order method used for the 3D transport equation can written as

$$\boldsymbol{U}_{n+1} - \tfrac{1}{2}\Delta t\left(\ \boldsymbol{G}_v^V(\boldsymbol{U}_{n+1}) + \boldsymbol{G}_v^V(\boldsymbol{U}_n)\right) = \boldsymbol{U}_n + \Delta t\ \boldsymbol{G}_h(\boldsymbol{U}_n) + \Delta t\ \boldsymbol{G}_v^I(\boldsymbol{U}_n) \tag{3.24}$$

The horizontal terms and the vertical convective terms are integrated using a first order explicit Euler method and the vertical viscous terms are integrated using a second order implicit trapezoidal rule. The higher order method can be written

$$\begin{aligned} \boldsymbol{U}_{n+1/2} - \tfrac{1}{4}\Delta t\ \left(\boldsymbol{G}_v^V(\boldsymbol{U}_{n+1/2}) + \boldsymbol{G}_v^V(\boldsymbol{U}_n)\right) = \\ \boldsymbol{U}_n + \tfrac{1}{2}\Delta t\ \boldsymbol{G}_h(\boldsymbol{U}_n) + \tfrac{1}{2}\Delta t\ \boldsymbol{G}_v^I(\boldsymbol{U}_n) \\ \boldsymbol{U}_{n+1} - \tfrac{1}{2}\Delta t\ \left(\boldsymbol{G}_v^V(\boldsymbol{U}_{n+1}) + \boldsymbol{G}_v^V(\boldsymbol{U}_n)\right) = \\ \boldsymbol{U}_n + \Delta t\ \boldsymbol{G}_h(\boldsymbol{U}_{n+1/2}) + \Delta t\ \boldsymbol{G}_v^I(\boldsymbol{U}_{n+1/2}) \end{aligned} \tag{3.25}$$

The horizontal terms and the vertical convective terms are integrated using a second order Runge Kutta method and the vertical terms are integrated using a second order implicit trapezoidal rule for the vertical terms.

3.3 Boundary Conditions

3.3.1 Closed boundaries

Along closed boundaries (land boundaries), normal fluxes are forced to zero for all variables. For the momentum equations, this leads to full-slip along land boundaries. For the shallow water equations, the no slip condition can also be applied where both the normal and tangential velocity components are zero.

3.3.2 Open boundaries

For the shallow water equations a number of different boundary conditions can be applied

The flux, velocity and Flather boundary conditions are all imposed using a weak approach. A ghost cell technique is applied where the primitive variables in the ghost cell are specified. The water level is evaluated based on the value of the adjacent interior cell, and the velocities are evaluated based on the boundary information. For a discharge boundary, the transverse velocity is set to zero for inflow and passively advected for outflow. The boundary flux is then calculated using an approximate Riemann solver.

The Flather (1976) condition is one of the most efficient open boundary conditions. It is very efficient in connection with downscaling coarse model simulations to local areas (see Oddo and Pinardi (2007)). The instabilities, which are often observed when imposing stratified density at a water level boundary, can be avoided using Flather conditions

The level boundary is imposed using a strong approach based on the characteristic theory (see e.g. Sleigh et al., 1998).

The discharge boundary condition is imposed using both a weak formulation using ghost cell technique described above and a strong approach based on the characteristic theory (see e.g. Sleigh et al., 1998).

Note that using the weak formulation for a discharge boundary the effective discharge over the boundary may deviate from the specified discharge.

For transport equations, either a specified value or a zero gradient can be given. For specified values, the boundary conditions are imposed by applying the specified concentrations for calculation of the boundary flux. For a zero gradient condition, the concentration at the boundary is assumed to be identical to the concentration at the adjacent interior cell.

3.3.3 Flooding and drying

The approach for treatment of the moving boundaries problem (flooding and drying fronts) is based on the work by Zhao et al. (1994) and Sleigh et al. (1998). When the depths are small the problem is reformulated and only when the depths are very small the elements/cells are removed from the calculation. The reformulation is made by setting the momentum fluxes to zero and only taking the mass fluxes into consideration.

The depth in each element/cell is monitored and the elements are classified as dry, partially dry or wet. Also the element faces are monitored to identify flooded boundaries.

- An element face is defined as flooded if the following two criteria are satisfied: Firstly, the water depth at one side of face must be less than a tolerance depth, h_{dry}, and the water depth at the other side of the face larger than a tolerance depth, h_{flood}. Secondly, the sum of the still water depth at the side for which the water depth is less than h_{dry} and the surface elevation at the other side must be larger than zero.

- An element is dry if the water depth is less than a tolerance depth, h_{dry}, and no of the element faces are flooded boundaries. The element is removed from the calculation.
- An element is partially dry if the water depth is larger than h_{dry} and less than a tolerance depth, h_{wet}, or when the depth is less than the h_{dry} and one of the element faces is a flooded boundary. The momentum fluxes are set to zero and only the mass fluxes are calculated.
- An element is wet if the water depth is greater than h_{wet}. Both the mass fluxes and the momentum fluxes are calculated.

The wetting depth, h_{wet}, must be larger than the drying depth, h_{dry}, and flooding depth, h_{flood}, must satisfy

$$h_{dry} < h_{flood} < h_{wet} \tag{3.26}$$

The default values are $h_{dry} = 0.005m$, $h_{flood} = 0.05m$ and $h_{wet} = 0.1m$.

Note, that for very small values of the tolerance depth, h_{wet}, unrealistically high flow velocities can occur in the simulation and give cause to stability problems.

4 Infiltration and Leakage

The effect of infiltration and leakage at the surface zone may be important in cases of flooding scenarios on otherwise dry land. It is possible to account for this in one of two ways: by Net infiltration rates or by constant infiltration with capacity.

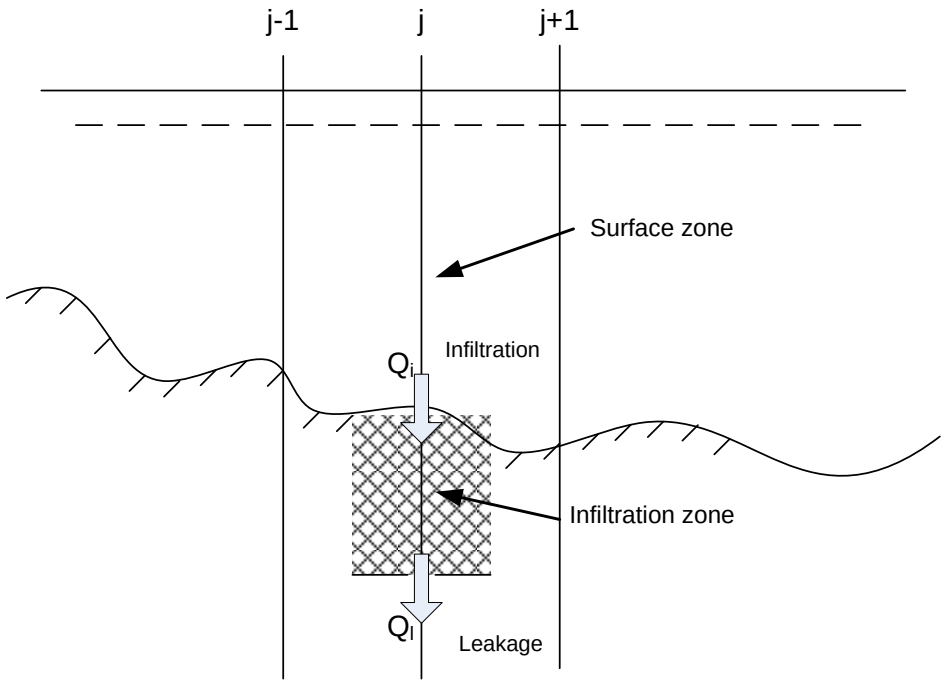

Figure 4.1 Illustration of infiltration process

4.1 Net Infiltration Rates

The net infiltration rate is defined directly. This will act as a simple sink in each element in the overall domain area.

The one-dimensional vertical continuity equation is solved at each hydrodynamic time step after the two-dimensional horizontal flow equations have been solved. The calculation of the new water depth in the free surface zone for each horizontal element is found by

$$H(j) = H(j) - V_{infiltration}(j) \,/A(j) \tag{4.1}$$

Where $V_{infiltration}(j)$ is the infiltrated volume in element (j) and A(j) the area of the element.

If $H(j)$ becomes marked as *dry* then element (j) will be taken out of the two-dimensional horizontal flow calculations and no infiltration can occur until the element is flooded again.

In summary: when using Net infiltration rate an unsaturated zone is never specified and thus has no capacity limits, so the specified infiltration rates will always be fully effectuated as long as there is enough water available in the element.

4.2 Constant Infiltration with Capacity

Constant infiltration with capacity describes the infiltration from the free surface zone to the unsaturated zone and from the unsaturated zone to the saturated zone by a simplified model. The model assumes the following:

- The unsaturated zone is modelled as an infiltration zone with constant porosity over the full depth of the zone.
- The flow between the free surface zone and the infiltration zone is based on a constant flow rate, i.e. $V_{infiltration} = Q_i \cdot \Delta t$ where Q_i is the prescribed flow rate.
- The flow between the saturated and unsaturated zone is modelled as a leakage Q_l having a constant flow rate, i.e. $V_{leakage} = Q_l \cdot \Delta t$.

The simplified model described above is solved through a one-dimensional continuity equation. Feedback from the infiltration and leakage to the two-dimensional horizontal hydrodynamic calculations is based solely on changes to the depth of the free surface zone – the water depth.

Note that the infiltration flow cannot exceed the amount of water available in the free surface water zone nor the difference between the water capacity of the infiltration zone and the actual amount of water stored there. It is possible that the infiltration flow completely drains the free surface zone from water and thus creates a dried-out point in the two-dimensional horizontal flow calculations.

The one-dimensional vertical continuity equation is solved at each hydrodynamic time step after the two-dimensional horizontal flow equations have been solved. The solution proceeds in the following way:

1. Calculation of the volume from leakage flow in each horizontal element – $V_{leakage}(j)$

$$V_{leakage}(j) = Q_l(j) \cdot \Delta t \cdot A(j) \tag{4.2}$$

$$V_{leakage}(j) = \min(V_{leakage}(j), V_i(j)) \tag{4.3}$$

$$V_i(j) := V_i(j) - V_{leakage}(j) \tag{4.4}$$

   Where $V_i(j)$ is the total amount of water in the infiltration zone and $Q_l(j)$ is the leakage flow rate.

2. Calculation of the volume from infiltration flow in each horizontal element – $V_{infiltration}(j)$

$$V_{infiltration}(j) = Q_i(j) \cdot \Delta t \cdot A(j) \tag{4.5}$$

$$V_{infiltration}(j) = \min\left(V_{infiltration}(j), SC_i(j) - V_i(j), H(j) \cdot A(j)\right) \tag{4.6}$$

$$V_i(j) := V_i(j) + V_{infiltration}(j) \tag{4.7}$$

   Where $Q_i(j)$ is the infiltration rate, $SC_i(j)$ is the water storage capacity and $H(j)$ the depth of the free surface.

3. Calculation of the new water depth in the free surface zone for each horizontal element

$$H(j) = H(j) - V_{infiltration}(j)/A(j) \quad (4.8)$$

If $H(j)$ becomes marked as *dry* then element *(j)* will be taken out of the two-dimensional horizontal flow calculations. The element can still *leak* but no infiltration can occur until the element is flooded again.

The water storage capacity of the infiltration zone is calculated as

$$SC_i(j) = Z_i(j) \cdot A(j) \cdot \gamma(j) \quad (4.9)$$

Where $Z_i(j)$ is the depth of the infiltration zone and $\gamma(j)$ is the porosity of the same zone.

In summary, when using Constant infiltration with capacity there can be situations where the picture is altered and the rates are either only partially effectuated or not at all:

- If $= H(j) < H_{dry}$ on the surface (dry surface) => infiltration rate is not effectuated
- If: the water volume in the infiltration zone reaches the full capacity => infiltration rate is not effectuated
- If: the water volume is zero in the infiltration zone (the case in many initial conditions) => leakage rate is not effectuated
- Leakage volume must never eclipse the available water volume in the infiltration zone, if so we utilise the available water volume in infiltration zone as leakage volume
- Infiltration volume must never eclipse the available water volume on the surface, if so we utilise the available water on the surface as infiltration volume

5 Jet Sources

The simulation of jets/plumes is based on dynamic coupling of nearfield integrated jet solution and the farfield hydrodynamic flow model (MIKE 3 Flow Model FM).

5.1 Nearfield Calculations

The near field solution is based on the integral jet model equations described by Jirka (2004). It determines the steady state solution of the jet/plume by solving conservation equations for flux and momentum, salinity and temperature (if included) under the given ambient conditions.

The velocity profile and distribution of state parameters and scalar mass is assumed to follow the Gaussian formulation. The jet model employs an entrainment closure approach that distinguishes between the separate contributions of transverse shear and of azimuthal shear mechanisms. It further contains a quadratic law turbulent drag force mechanism (F_D) as suggested by a number of recent detailed experimental investigations on the dynamics of transverse jets into crossflow. The conservation principles for volume (continuity), momentum components in the global directions, state parameters and scalar mass, follow Jirka (2004), lead to the equations below:

$$\frac{dQ}{ds} = E \tag{5.1}$$

$$\frac{dM_x}{ds} = Eu_a + F_D\sqrt{1 - cos^2\theta cos^2\sigma} \tag{5.2}$$

$$\frac{dM_y}{ds} = -F_D \frac{cos^2\theta sin\sigma cos\sigma}{\sqrt{1 - cos^2\theta cos^2\sigma}} \tag{5.3}$$

$$\frac{dM_z}{ds} = \pi\lambda^2 b^2 g_c' - F_D \frac{sin\theta cos\theta cos\sigma}{\sqrt{1 - cos^2\theta cos^2\sigma}} \tag{5.4}$$

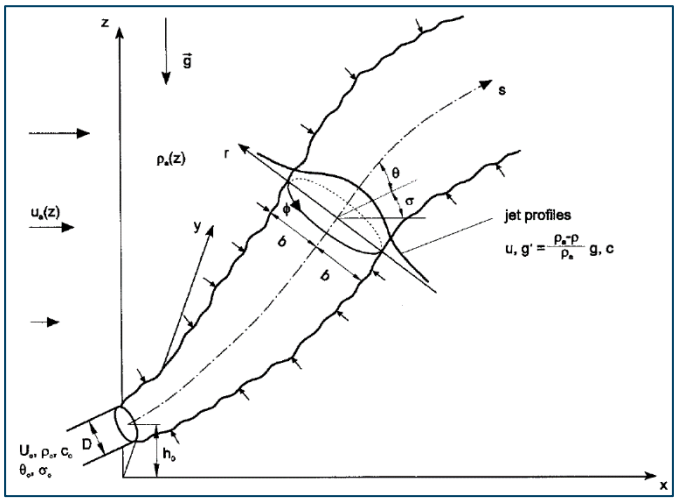

Figure 5.1 Nearfield jet integral model definition sketch

Where s is the axial distance along the jet trajectory and E is the rate of entrainment, and b is the characteristic width of the jet, which is defined as the jet radius, where the jet excess velocity is $e^{-1} = 37\%$. The centerline density is contained in the definition of centerline buoyancy g_c' and is calculated by the UNESCO equation of state, as function of salinity (S) and temperature (T):

$$\rho_{Jet} = \rho_{UNESCO}(S,T) \tag{5.5}$$

If sediments are present inside the jet, and their dynamics are included in the calculations, then the jet density will be corrected for the presence of sediments. This can be activated by defining the source in MT module and activating the MT-HD feedback.

$$\rho_{Jet} = (1 - C_{sed})\rho_{Jet} + C_{sed}\rho_{sed} \tag{5.6}$$

C_{sed} is the volumetric sediment concentration derived from the sediment concentration provided by the user for the Jet source in MT module, and ρ_{sed} is the sediment density provided by the user for the MT-HD feedback in MT module.
The buoyant acceleration is then defined as below, where $\rho_a$is the ambient density, and ρ_{ref} is the reference density calculated by the reference salinity and temperatures provided by the user in HD module.

$$g_c' = \frac{\rho_{Jet} - \rho_a}{\rho_{ref}} g \tag{5.7}$$

The two important physical processes influencing the jet trajectory and dilution rates are the entrainment rate (E) and the ambient drag force (F_D). The entrainment rate is calculated as being proportional to the streamwise contribution of the jet centerline velocity (u_c) plus the azimuthal contribution from the transverse component of the ambient velocity ($u_a\sqrt{1 - cos^2\theta cos^2\sigma}$).

$$E = 2\pi b u_c \left(\alpha_1 + \alpha_2 \frac{sin\theta}{F_l^2} + \alpha_3 \frac{u_a cos\theta cos\sigma}{u_c + u_a}\right) + 2\pi b u_a \sqrt{1 - cos^2\theta cos^2\sigma}\,\alpha_4 |cos\theta cos\sigma| \tag{5.8}$$

F_l is the local densimetric Froude number, and is defined as:

$$F_l = \frac{u_c}{\sqrt{g_c' b}} \tag{5.9}$$

The first term in the streamwise part of the entrainment function represents the “pure jet” effects, the second term adds the effect of “pure plume” and the third term is for “pure wake”. The four coefficients defining the entrainment rate are given the empirical values suggested by Jirka (2004):

$$\alpha_1 = 0.055 \;,\; \alpha_2 = 0.6 \;,\; \alpha_3 = 0.055 \;,\; \alpha_4 = 0.5 \tag{5.10}$$

Deflection of the jet is a consequence of the pressure drag exerted on it by the cross flow (F_D) and of the entrainment by the jet of laterally moving fluid from the crossflow (Eu_a). The drag force is parametrized as a quadratic law force mechanism (Jirka, 2004):

$$F_D = \frac{1}{2} C_D 2\sqrt{2} b u_a^2 (1 - cos^2\theta cos^2\sigma) \tag{5.11}$$

The jet diameter is calculated as $2\sqrt{2}b$ and C_D is the drag coefficient as function of velocity ratio between jet and the ambient, following Chan et al. (1976).

Calculations of the jet trajectory are discretized based on the incremental distance along the jet trajectory (ds). Following a recommendation from Lee and Cheung (1990), the spatial discretization of jet trajectory is calculated as below:

$$ds = dt(u_c + u_a cos\theta cos\sigma) \tag{5.12}$$

Where

$$dt = \frac{0.1D}{u_c}$$

However, the value of dt is set to have cut-off values of 0.001 seconds and 1.0 seconds. D is the initial jet diameter.

This jet (nearfield) model calculates the jet trajectory and dilution until it reaches the end of nearfield region. This is done at each HD time-step in the background flow model. Although the HD time-steps can be much smaller than the time it takes for the trajectory to reach the end of nearfield region, it is assumed that the temporal variations in the background flow (ambient) are slower than the time it takes for the jet to go from discharge point to the point of farfield release.

5.2 End of Nearfield region

In general, where the jet loses its driving characteristics over the ambient flow (momentum and buoyancy), it has reached the end of its nearfield region and its volume and scalar mass can be transferred and dispersed by the ambient flow into the Farfield region. This can happen under different circumstances:

- **Jet in cross-flow**: The jet momentum M is combination of its initial momentum at the diffuser, buoyancy and the ambient flow induced (co- or opposing) momentum $\mathrm{M_a}$. It loses its driving characteristics over the ambient flow when the excess momentum becomes small, and close to the ambient flow momentum. This can be considered as the end of the nearfield region and the release into the Farfield model by following the condition: $\mathrm{M} - \mathrm{M_a} < \varepsilon.\mathrm{M_a}$, where epsilon ε is left as a user-defined/calibration parameter, with default value of 1%.

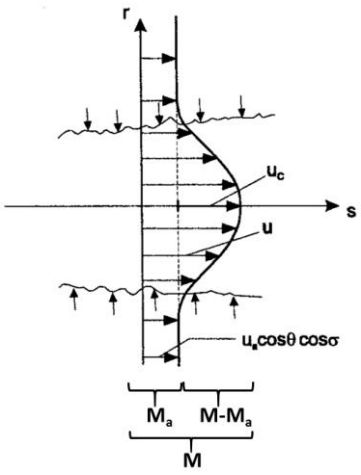

Figure 5.2 Illustration of the jet velocity field and the contribution from the ambient flow (Modified image from Jirka, 2004)

- **Jet in stagnant environment**: Under stagnant conditions, the contribution from the ambient currents to the jet momentum is zero, and the Nearfield region can extend until the point where the jet loses its own momentum due to dilution and buoyancy. Considering the modeling/numerical limitations, a minimum value for the jet excess velocity can be defined (gamma γ) to mark the end of Nearfield region and the release into Farfield model. The default value for gamma is set to 1 cm/s.
- **Jet in stratified stagnant environment**: Non-horizontal jets (positively buoyant jets pointed downward or negatively buoyant jets pointed upward) in stagnant stratification create a complex situation. Depending on the stratification gradient and the jet initial momentum, the jet can either be trapped in a layer where its density equals the ambient density, or it overshoots and experiences a reversed buoyancy. In latter case, the jet experiences a lateral collapse in form of an internal density current formation in opposite direction and it ends up trapped in a terminal density level. These complex processes are not included in the integral jet model formulation and – in the absence of an adequate transition cut-off- it predicts (unrealistically) an infinite number of oscillations about the terminal level. Therefore, the second buoyancy reversal in the jet calculations is considered as the end of Nearfield calculations and the release into the Farfield model.
- **Jet in strong opposing flow**: Jet integral models cannot be expected to hold for flow situations in which boundary layer behavior is no longer maintained. The boundary layer approximation implies a pressure within the jet equal to that in the outside ambient. This is violated whenever the jet exhibits strong curvature such as going into strong opposing ambient current. Therefore, the jet nearfield solution stops and releases into Farfield model as soon as it experiences a strong opposing flow.

The other criterion that ends the nearfield calculations is when the jet reaches the bottom, surface or a lateral boundary. The dynamics of the jet approaching a solid boundary or water surface are not yet included in the nearfield calculations of the MIKE jet module. Among the impacts are variations in entrainment rates at the vicinity of the boundary. The nearfield calculations continue un-influenced until the jet reaches the boundary, and there it releases into the Farfield model.

5.3 Nearfield-Farfield model coupling

The coupling between the Nearfield and Farfield model concerns both the reading of ambient conditions as an input for the Nearfield jet model, and the release of jet discharge into the Farfield flow model at the end of the Nearfield region.

The ambient flow conditions can be determined either as the local flow conditions at the jet location or as the upstream ambient flow conditions. The upstream option can be used to avoid unrealistic feedback between the jet solution and the ambient flow in cases with dominant advection effects on the released material from the ambient flow. For the upstream ambient flow condition, the conditions are obtained at a point defined by distance from the jet location in the upstream flow direction. The distance is the maximum of the characteristic length determined from the mesh and a user-specified minimum upstream distance. The characteristic length is here determined as 2.3 times the square root of the local element area at the initial release point.

At the end of Nearfield region (determined by any of conditions described in previous section), the final jet discharge (which is diluted) is released into the Farfield flow model at the corresponding point in space. This will assure that the right volume with right dilution is released into the Farfield model at the right location. The discharge is distributed into several sources over a plane area corresponding to the final jet diameter and with a Gaussian distribution for volume and other scalars. The number of sources depend on the mesh resolution in the Farfield model.

The increased jet discharge at the end of the Nearfield region (due to entrainment) is inserted into the Farfield flow model at each Hydrodynamic time-step, which then impacts the hydrodynamic solution at the next time step. The shallow-water equations being solved in the Farfield flow model may not be able to correctly handle the insertion and acceleration of such relatively large volume inserted into the domain (this depends as well on local mesh resolution and water depth). The resulting flow field therefore might not appear realistic. As a partial remedy, and to help the solution, at each of the release point sources there will be added a forcing (momentum flux) to the momentum equation, in the direction of jet release into the ambient domain, calculated as:

$$F_x = M \cos\theta \cos\sigma,\ F_y = M \cos\theta \sin\sigma \tag{5.13}$$

The increased jet discharge and (consequently) its dilution at the release point is a result of entrainment along its trajectory. Conservation of mass and volume in the Farfield flow model then requires removing this excess mass and volume that have been inserted at the release point. This has been done by introducing entrainment sinks along the centerline of the jet trajectory (see Figure 5.3). The number of sinks depend on the mesh resolution in the Farfield model. This method follows the Distributed Entrainment Sink Approach (DESA) proposed by Choi and Lee (2007).

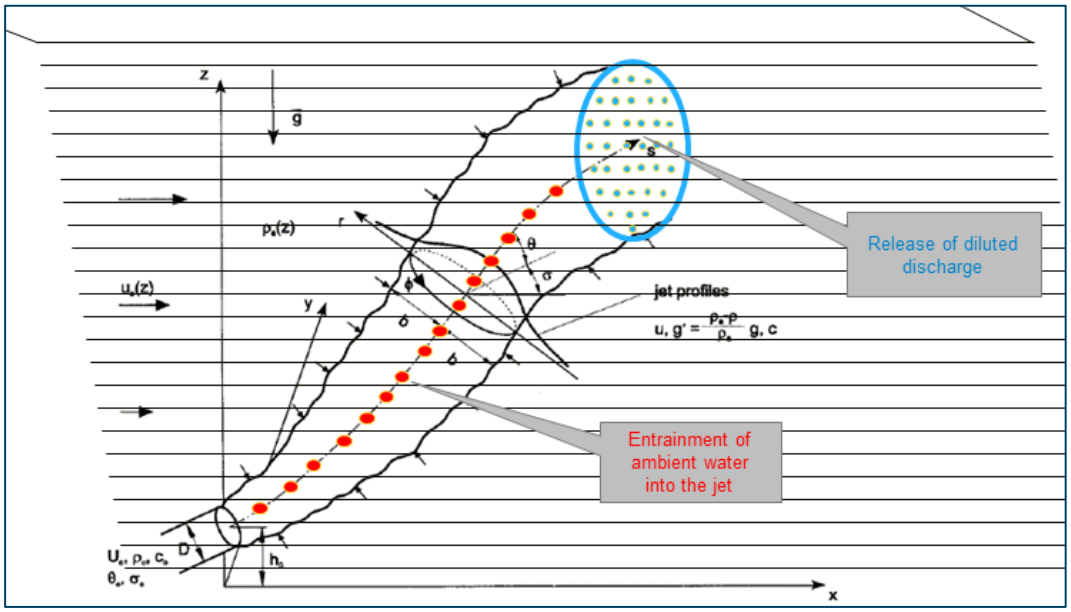

Figure 5.3 Illustration of positioning of entrainment sinks along the trajectory in a 3D domain, and the distributed source points at the release location

Similar to the problem at the release point, at the sink locations, subtraction of volume inside the domain may result in dubious flow fields near the sinks (depending on local mesh resolution). Therefore, following the same reasoning used for the release point, at each sink point, a forcing (momentum flux), calculated as the product of sink rate and the ambient flow velocity, is added to the momentum balance with an opposing direction. This cannot be effective for the vertical velocities induced by the sinks, where their impact becomes more visible in vertical jets.

(5.14)

$$f_x = -q_{sink} u_{a\_x} \quad , \quad f_y = -q_{sink} u_{a\_y}$$

6 Validation

The new finite-volume model has been successfully tested in a number of basic, idealised situations for which computed results can be compared with analytical solutions or information from the literature. The model has also been applied and tested in more natural geophysical conditions; ocean scale, inner shelves, estuaries, lakes and overland, which are more realistic and complicated than academic and laboratory tests. A detailed validation report is under preparation.

This chapter presents a comparison between numerical model results and laboratory measurements for a dam-break flow in an L-shaped channel.

Additional information on model validation and applications can be found here:

http://www.mikepoweredbydhi.com/download/product-documentation

6.1 Dam-break Flow through Sharp Bend

The physical model to be studied combines a square-shaped upstream reservoir and an L-shaped channel. The flow will be essentially two-dimensional in the reservoir and at the angle between the two reaches of the L-shaped channel. However, there are numerical and experimental evidences that the flow will be mostly unidimensional in both rectilinear reaches. Two characteristics or the dam-break flow are of special interest, namely

- The "damping effect" of the corner
- The upstream-moving hydraulic jump which forms at the corner

The multiple reflections of the expansion wave in the reservoir will also offer an opportunity to test the 2D capabilities of the numerical models. As the flow in the reservoir will remain subcritical with relatively small-amplitude waves, computations could be checked for excessive numerical dissipation.

6.1.1 Physical experiments

A comprehensive experimental study of a dam-break flow in a channel with a 90 bend has been reported by Frazão and Zech (2002, 1999a, 1999b). The channel is made of a 3.92 and a 2.92 metre long and 0.495 metre wide rectilinear reaches connected at right angle by a 0.495 x 0.495 m square element. The channel slope is equal to zero. A guillotine-type gate connects this L-shaped channel to a 2.44 x 2.39 m (nearly) square reservoir. The reservoir bottom level is 33 cm lower that the channel bed level. At the downstream boundary a chute is placed. See the enclosed figure for details.

Frazão and Zech performed measurements for both dry bed and wet bed condition. Here comparisons are made for the case where the water in the reservoir is initially at rest, with the free surface 20 cm above the channel bed level, i.e. the water depth in the reservoir is 53 cm. The channel bed is initially dry. The Manning coefficients evaluated through steady-state flow experimentation are 0.0095 and 0.0195 $s/m^{1/3}$, respectively, for the bed and the walls of the channel.

The water level was measured at six gauging points. The locations of the gauges are shown in Figure 6.1 and the coordinates are listed in Table 6.1.

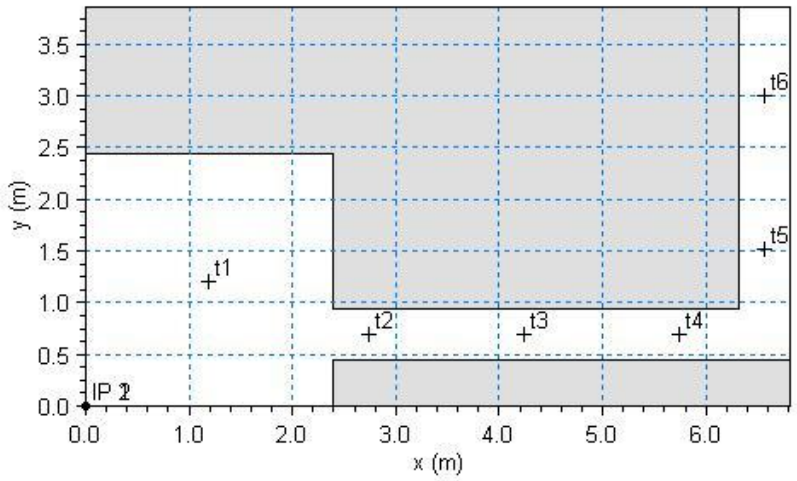

Figure 6.1 Set-up of the experiment by Frazão and Zech (2002)

Table 6.1 Location of the gauging points

Location	x (m)	y (m)
T1	1.19	1.20
T2	2.74	0.69
T3	4.24	0.69
T4	5.74	0.69
T5	6.56	1.51
T6	6.56	3.01

6.1.2 Numerical experiments

Simulations are performed using both the two-dimensional and the three-dimensional shallow water equations.

An unstructured mesh is used containing 18311 triangular elements and 9537 nodes. The minimum edge length is 0.01906 m and the maximum edge length is 0.06125 m. In the 3D simulation 10 layers is used for the vertical discretization. The time step is 0.002 s. At the downstream boundary, a free outfall (absorbing) boundary condition is applied. The wetting depth, flooding depth and drying depth are 0.002 m, 0.001 m and 0.0001 m, respectively.

A constant Manning coefficient of 105.26 $m^{1/3}/s$ is applied in the 2D simulations, while a constant roughness height of $5 \cdot 10^{-5}$ m is applied in the 3D simulation.

6.1.3 Results

In Figure 6.2 time series of calculated surface elevations at the six gauges locations are compared to the measurements. In Figure 6.3 contour plots of the surface elevations are shown at T = 1.6, 3.2 and 4.8 s (two-dimensional simulation).

In Figure 6.4 a vector plot and contour plots of the current speed at a vertical profile along the centre line (from (x,y)=(5.7, 0.69) to (x,y)=(6.4, 0.69)) at T = 6.4 s is shown.

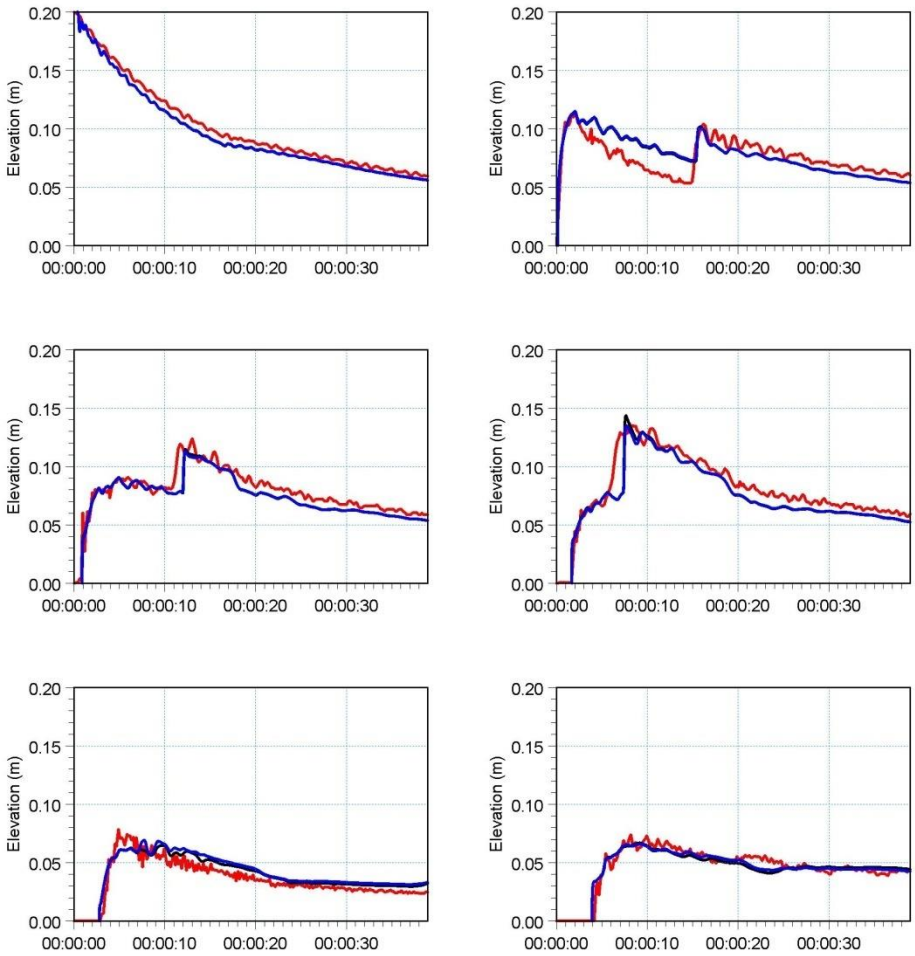

Figure 6.2 Time evolution of the water level at the six gauge locations. (blue) 3D calculation, (black) 2D calculation and (red) Measurements by Frazão and Zech (1999a,b)

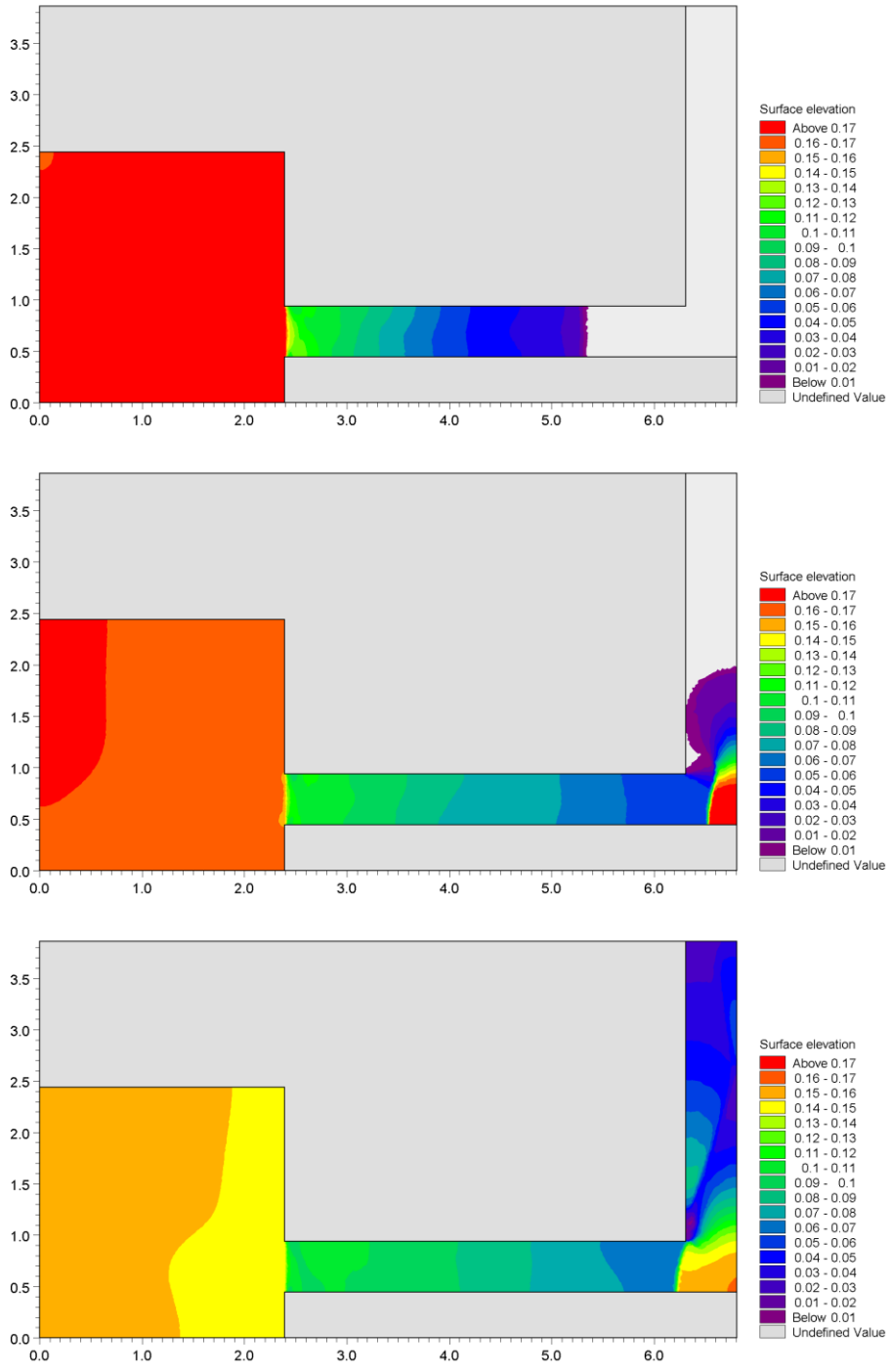

Figure 6.3 Contour plots of the surface elevation at T = 1.6 s (top), T = 3.2 s (middle) and T = 4.8 s (bottom).

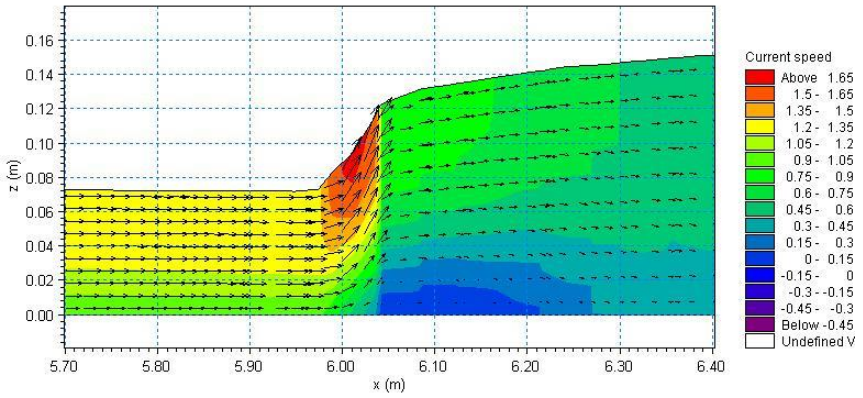

Figure 6.4 Vector plot and contour plots of the current speed at a vertical profile along the centre line at T = 6.4 s

6.2 Jet Source

Fan (1967) did comprehensive series of laboratory tests, where a negatively buoyant jet is discharged vertically down into a crossflow and into a stagnant stratified water tank. Figure 6.5 shows a photograph of the negatively buoyant jet in crossflow test 40-8-D, which is used to validate the MIKE jet model.

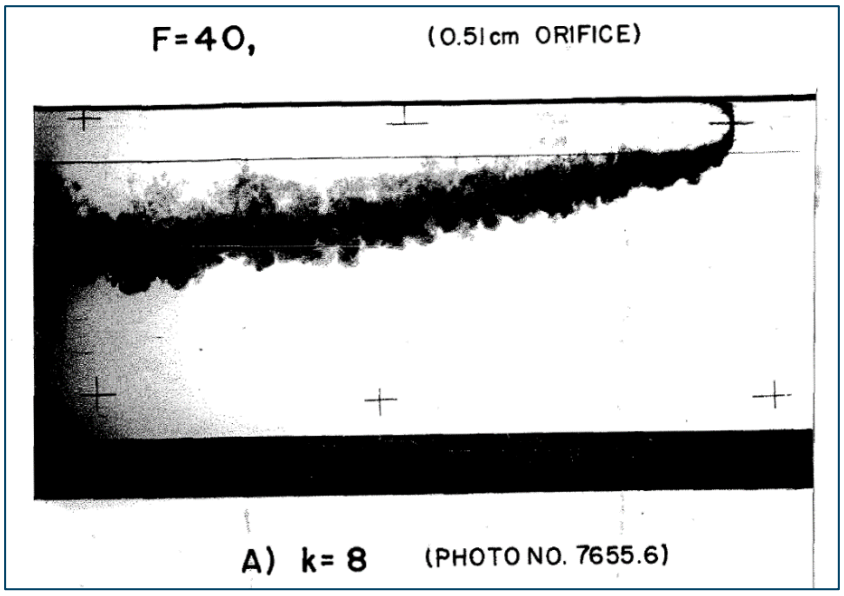

Figure 6.5 Photograph of test 40-8-D (Fan, 1967)

In Figure 6.6, the jet centreline trajectory (solid blue line) and the corresponding characteristic width (dash blue line) calculated by the MIKE integral jet model are plotted upon the lab observations reported by Fan (the background image) of test number 40-8D. The trajectory and the general width of the jet follows the observations very well. The Farfield results of the same simulation are shown in Figure 6.7, where the Nearfield calculations also are indicated.

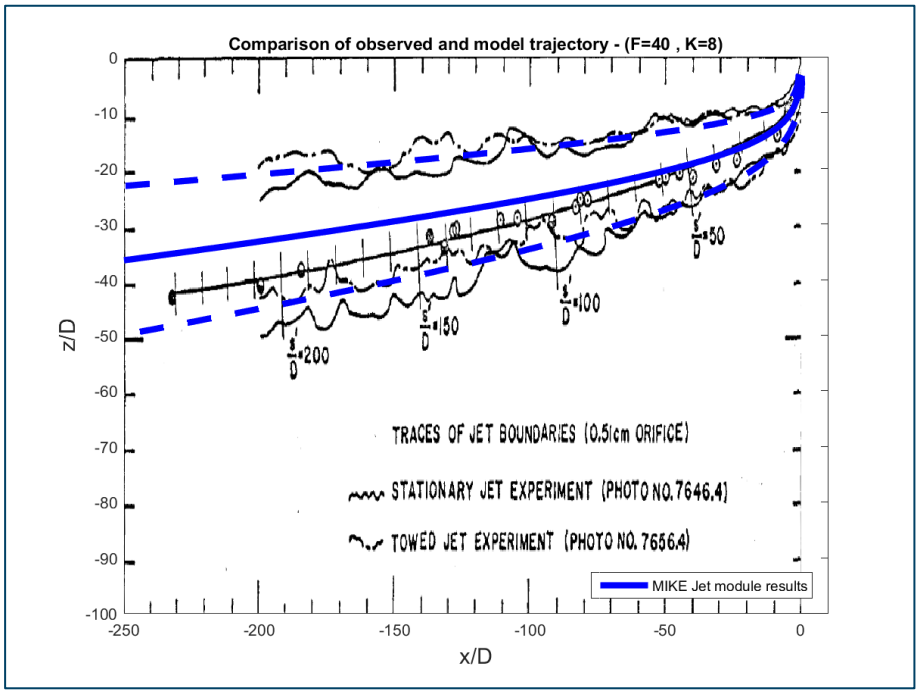

Figure 6.6 Comparison of observed (Fan, 1967) and model results of nearfield jet trajectory

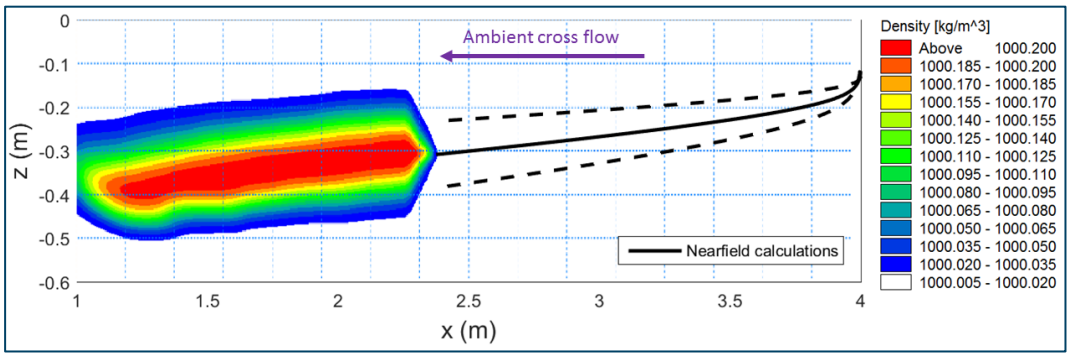

Figure 6.7 Presentation of the Nearfield calculations over the Farfield flow model MIKE 3 FM results

Besides the jet-in-crossflow tests, Fan did also tests where the negatively buoyant jet is discharged into a stagnant stratified environment. These tests demonstrated the complicated process of jet overshooting its neutral density level and experiencing a reversed buoyancy and finally being trapped in a new density level. The jet integral equations do not resolve all the physical details of this phenomenon, but can estimate the trajectory path and dilution rates well.

In Figure 6.8, the jet centreline trajectory (solid blue line) and the corresponding characteristic width b (dash blue line) calculated by the integral jet model are plotted upon the lab observations of Fan (stratified tank test 1) and the CorJet model results (single-jet module in CORMIX) as the background image (from Jirka 2004). The trajectory and the general width of the jet follows both the CoreJet results and the observations very well. Due to ambient stratification and the jet momentum, the jet overshoots its neutral density layer and experiences a buoyancy reversal (BR). The nearfield calculations has ceased after the second BR.

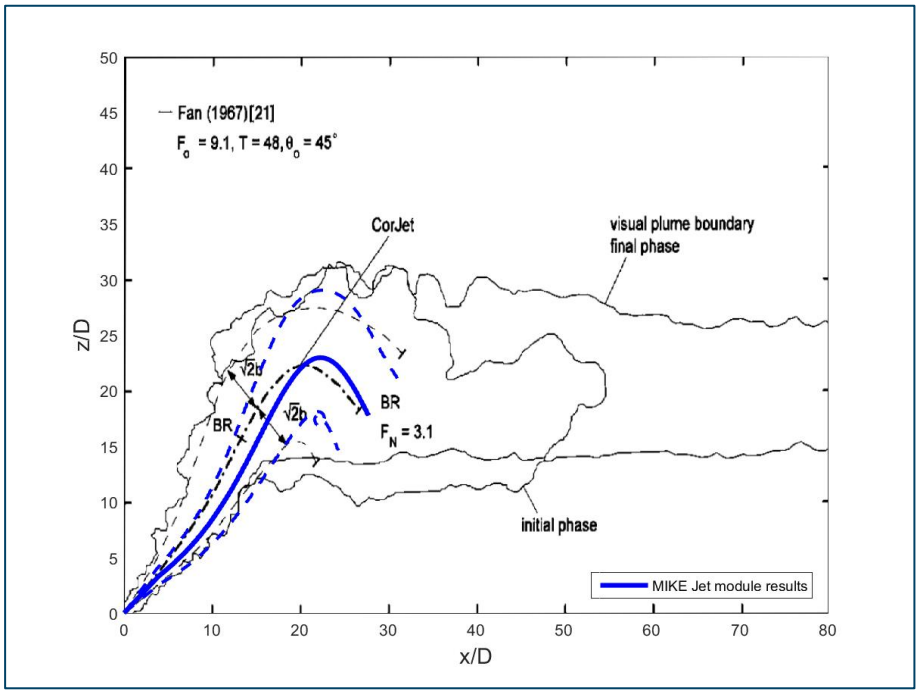

Figure 6.8 Comparison of MIKE Nearfield model results with observed visual plume (Fan 1967) and CorJet (Jirka 2004)

Jirka (2004) compared the CoreJet model results to few other test cases from Fan's laboratory experiment. The same cases have been simulated by MIKE jet module and the results are plotted in Figure 6.9 upon the graphs presented by Jirka (2004). The general agreement with both the measured values and the CoreJet model results are satisfactory.

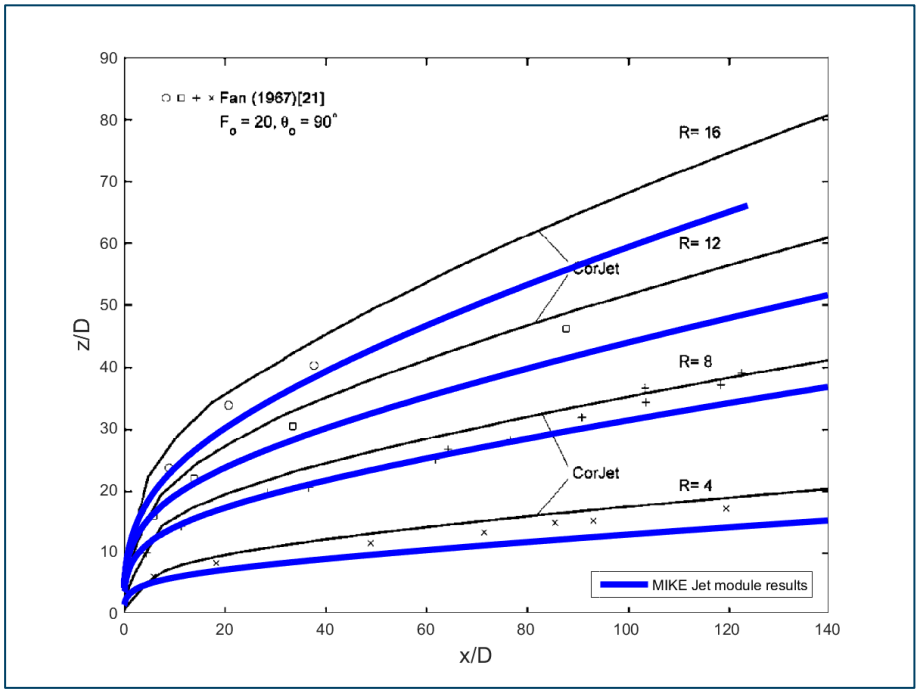

Figure 6.9 Comparison of MIKE Jet module results with integral model predictions of Jirka (2004) with experimental data of Fan (1967)

In jets that contain sediments with high levels of concentration, the weight of sediment should be included in the Nearfield calculations. By activating the HD/MT coupling feature, the sediment sources defined in the MT module will be taken into account when calculating the jet density in the Nearfield calculations.

Decrop et al. (2013) did a series of laboratory measurements of sediment mixture jets in cross flow. In Figure 6.10 a photograph of the laboratory experiment (with strong cross-flow) is shown. In Figure 6.11 and Figure 6.12 the results of MIKE jet module is compared with Decrop's measurements as well as Fisher (1979) and the Lagrangian model of Lee and Chu (2003).

Figure 6.10 Image of the negatively buoyant sediment plume in crosss flow (Decrop, 2013)

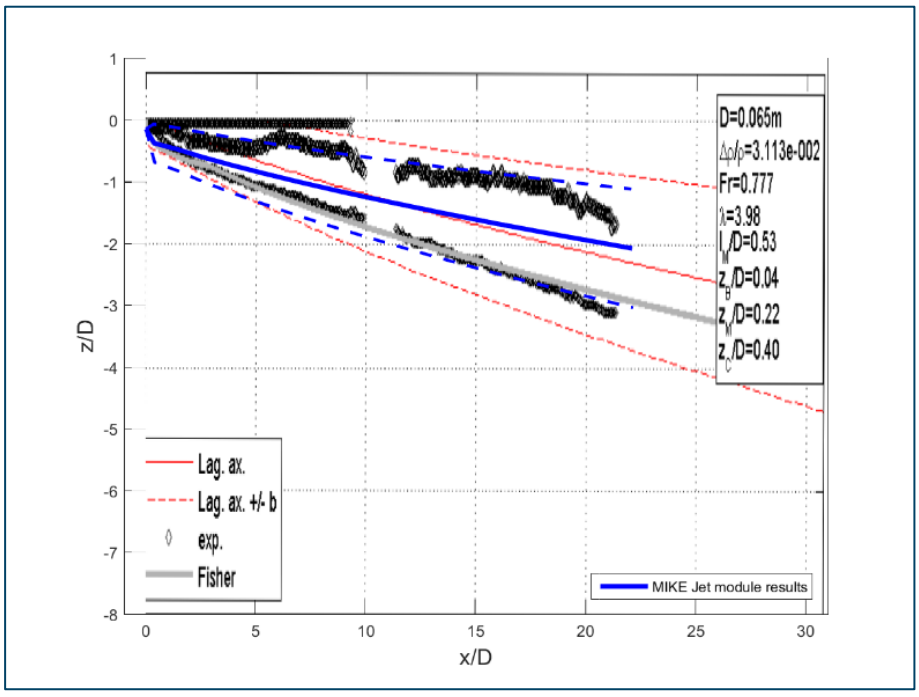

Figure 6.11 Comparison of the MIKE Jet module results with the experimental data of Decrop (2013) and other models

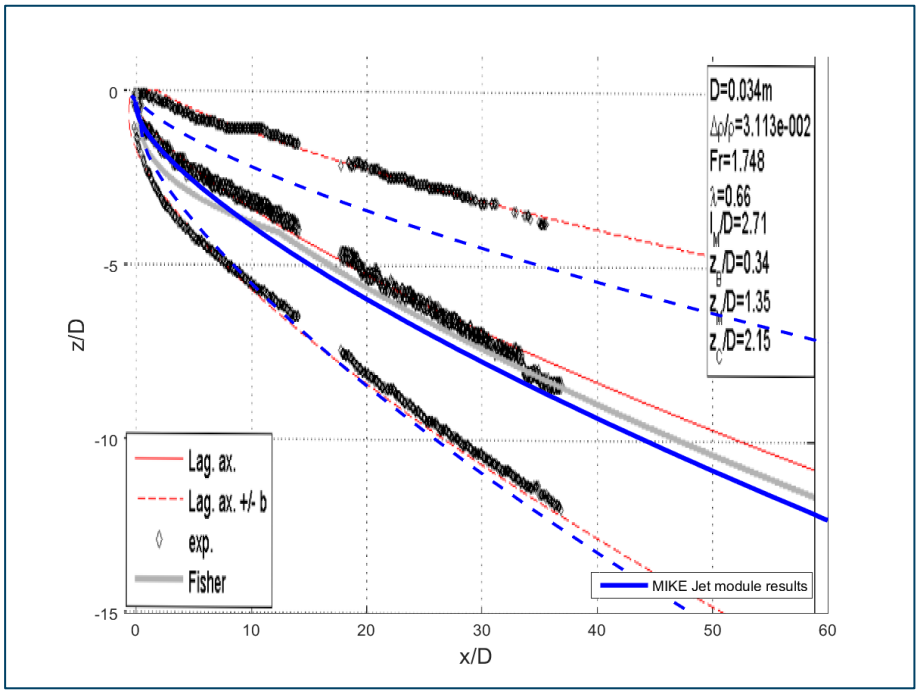

Figure 6.12 Comparison of the MIKE Jet module results with the experimental data of Decrop (2013) and other models

7 References

/1/ Chan, D.T.L., Kennedy, J.F. and Lin, J.T., 1976. Entrainment and drag forces of deflected jets. Journal of the Hydraulics Division, 102(5), pp.615-635.

/2/ Choi, K.W. and Lee, J.H., 2007. Distributed Entrainment Sink Approach (DESA)-a New Method for Modelling Mixing and Transport in the Intermediate Field.

/3/ Darwish M.S. and Moukalled F. (2003), TVD schemes for unstructured grids, Int. J. of Heat and Mass Transfor, 46, 599-611)

/4/ Decrop, B., Mulder, T. De & Troch, P., 2013. Experimental investigation of negatively buoyant sediment plumes resulting from Dredging operations. CoastLab 2012, (3).

/5/ Fan, L.N., 1967. Turbulent buoyant jets into stratified or flowing ambient fluids.

/6/ Fischer, H.B., 1979. Mixing in Inland and Coastal Waters. Academic Press.

/7/ Fredsøe, J. (1984), Turbulent boundary layers in Combined Wave Current Motion. J. Hydraulic Engineering, ASCE, Vol 110, No. HY8, pp. 1103-1120.

/8/ Geernaert G.L. and Plant W.L (1990), Surface Waves and fluxes, Volume 1 – Current theory, Kluwer Academic Publishers, The Netherlands.

/9/ Hirsch, C. (1990). Numerical Computation of Internal and External Flows, Volume 2: Computational Methods for Inviscid and Viscous Flows, Wiley.

/10/ Iqbal M. (1983). An Introduction to solar Radiation, Academic Press.

/11/ Jawahar P. and H. Kamath. (2000). A high-resolution procedure for Euler and Navier-Stokes computations on unstructured grids, Journal Comp. Physics, 164, 165-203.

/12/ Jirka, G.H., 2004. Integral model for turbulent buoyant jets in unbounded stratified flows. Part I: Single round jet. Environmental Fluid Mechanics, 4(1), pp.1-56.

/13/ Jones, O., Zyserman, J.A. and Wu, Yushi (2014), Influence of Apparent Roughness on Pipeline Design Conditions under Combined Waves and Current, *Proceedings of the ASME 2014 33rd International Conference on Ocean, Offshore and Arctic Engineering*.

/14/ Kantha and Clayson (2000). Small Scale Processes in Geophysical Fluid flows, International Geophysics Series, Volume 67.

/15/ Lee, J.H. and Cheung, V.W., 1986. Inclined plane buoyant jet in stratified fluid. Journal of Hydraulic Engineering, 112(7), pp.580-589.

/16/ Lee, J.H. and Cheung, V., 1990. Generalized Lagrangian model for buoyant jets in current. Journal of Environmental Engineering, 116(6), pp.1085-1106.

/17/ Lee, J.H.W and Chu, V., 2003. Turbulent jets and Plumes: A Lagrangian approach. Kluwer, pp378.

/18/ Lind & Falkenmark (1972), Hydrology: en inledning till vattenressursläran, Studentlitteratur (in Swedish).

/19/ Munk, W., Anderson, E. (1948), Notes on the theory of the thermocline, Journal of Marine Research, 7, 276-295.

/20/ Oddo P. and N. Pinardi (2007), Lateral open boundary conditions for nested limited area models: A scale selective approach, Ocean Modelling 20 (2008) 134-156.

/21/ Pugh, D.T. (1987), Tides, surges and mean sea-level: a handbook for engineers and scientists. Wiley, Chichester, 472pp

/22/ Rodi, W. (1984), Turbulence models and their applications in hydraulics, IAHR, Delft, the Netherlands.

/23/ Rodi, W. (1980), Turbulence Models and Their Application in Hydraulics - A State of the Art Review, Special IAHR Publication.

/24/ Roe, P. L. (1981), Approximate Riemann solvers, parameter vectors, and difference-schemes, Journal of Computational Physics, 43, 357-372.

/25/ Sahlberg J. (1984). A hydrodynamic model for heat contents calculations on lakes at the ice formation date, Document D4: 1984, Swedish council for Building Research.

/26/ Shu C.W. (1997), Essentially Non-Oscillatory and Weighted Essenetially Non-Oscillatory Schemes for Hyperbolic Conservation Laws, NASA/CR-97-206253, ICASE Report No. 97-65, NASA Langley Research Center, pp. 83.

/27/ Sleigh, P.A., Gaskell, P.H., Bersins, M. and Wright, N.G. (1998), An unstructured finite-volume algorithm for predicting flow in rivers and estuaries, Computers & Fluids, Vol. 27, No. 4, 479-508.

/28/ Smagorinsky (1963), J. General Circulation Experiment with the Primitive Equations, Monthly Weather Review, 91, No. 3, pp 99-164.

/29/ Soares Frazão, S. and Zech, Y. (2002), Dam-break in channel with 90° bend, Journal of Hydraulic Engineering, ASCE, 2002, 128, No. 11, 956-968.

/30/ Soares Frazão, S. and Zech, Y. (1999a), Effects of a sharp bend on dam-break flow, Proc., 28th IAHR Congress, Graz, Austria, Technical Univ. Graz, Graz, Austria (CD-Rom).

/31/ Soares Frazão, S. and Zech, Y. (1999b), Dam-break flow through sharp bends – Physical model and 2D Boltzmann model validation, Proc., CADAM Meeting Wallingford, U.K., 2-3 March 1998, European Commission, Brussels, Belgium, 151-169.

/32/ UNESCO (1981), The practical salinity scale 1978 and the international equation of state of seawater 1980, UNESCO technical papers in marine science, 36, 1981.

/33/ Wu, Jin (1994), The sea surface is aerodynamically rough even under light winds, Boundary layer Meteorology, 69, 149-158.

/34/ Wu, Jin (1980), Wind-stress Coefficients over sea surface and near neutral conditions – A revisit, Journal of Physical. Oceanography, 10, 727-740.

/35/ Zhao, D.H., Shen, H.W., Tabios, G.Q., Tan, W.Y. and Lai, J.S. (1994), Finite-volume two-dimensional unsteady-flow model for river basins, Journal of Hydraulic Engineering, ASCE, 1994, 120, No. 7, 863-833.